Available online at www.sciencedirect.com
SCIENCE DIRECT®
Solid State Nuclear Magnetic Resonance 28 (2005) 204–224
Solid State Nuclear Magnetic Resonance
www.elsevier.com/locate/ssnmr

^{93}Nb NMR chemical shift scale for niobia systems

Olga B. Lapina[a,*], Dzhalil F. Khabibulin[a], Konstantin V. Romanenko[a], Zhehong Gan[b], Mikhail G. Zuev[c], Vladimir N. Krasil'nikov[c], Vladimir E. Fedorov[d]

[a]*Boreskov Institute of Catalysis, SB RAS, Prosp. Lavrentieva 5, 630090 Novosibirsk, Russian Federation*
[b]*NHMF Laboratory, Florida State University, CIMAR/NMR, Florida, USA*
[c]*Institute of Solid State Chemistry, UB RAS, Ekaterinburg GSP-145, 620219 Russian Federation*
[d]*Nikolaev Institute of Inorganic Chemistry, SB RAS, 630090 Novosibirsk, Russian Federation*

Received 21 June 2005; received in revised form 12 September 2005
Available online 10 October 2005

Abstract

^{93}Nb solid-state NMR spectra of a series of inorganic niobates with Nb in different oxygen coordination environments were measured. For all studied compounds the chemical shielding and quadrupole tensor parameters were determined using conventional and ultrahigh field NMR facilities, ultrahigh speed MAS, DQ STMAS, solid-echo and computer modeling. It has been demonstrated that the ^{93}Nb isotropic chemical shift is sensitive to the coordination number of Nb sites. For the first time the ^{93}Nb NMR chemical shift scale for NbO_x polyhedra in solid materials has been proposed: for four-coordinated Nb sites, the isotropic shifts occur from −650 to −950 ppm; five-coordinated Nb sites have the isotropic shifts in the range of –900 to –980 ppm; for six-coordinated Nb sites the isotropic shifts vary from −900 to −1360 ppm; the shifts from −1200 to −1600 ppm are typical for seven-coordinated Nb sites; for eight-coordinated Nb sites the shifts are higher than −1400 ppm. The possible correlation between the value of the isotropic chemical shift and the ionic character of the NbO_x–MO_y polyhedra association has been suggested. The magnitude of the ^{93}Nb quadrupole coupling constant depends on the local symmetry of Nb sites and may vary from hundreds of kHz to hundreds of MHz.

Keywords: ^{93}Nb NMR; Solid-state NMR; Chemical shift scale; Niobates; High field MAS; STMAS

1. Introduction

Two recent symposia on Group Five Compounds have shown growing interest in niobium-based systems and their possible applications in heterogeneous catalysis [1–3]. This interest is driven in many respects by unique chemical properties of niobium compounds, not typical for other Group Five elements. For example, even a small amount of niobium oxide added to a known catalyst may considerably enhance its catalytic activity, selectivity and long-term stability [3]. Niobium (V) oxide and mixed oxides (Nb_2O_5–SiO_2, Nb_2O_5–Al_2O_3, Nb_2O_5–TiO_2, Nb_2O_5–V_2O_5, etc.) are often used as supports for metals or other metal-oxide catalysts [1–3]. Nb-containing mixed metal-oxide catalysts, e.g. MoVNbTeO, exhibit high activity and selectivity in conversion of light alkanes [3]. Hydrated niobium pentoxide (niobic acid, $Nb_2O_5 \cdot nH_2O$) and niobium phosphate have unusual high surface acidity and have shown significant catalytic activity, selectivity, and stability in acid-catalyzed reactions [3]. Many layered compounds containing niobium combined with other metals demonstrate photocatalytic activity [3].

This growing interest in niobium-based catalytic systems can explain most recent advances in spectroscopic techniques used for their characterization [4]. This does not include, however, solid-state ^{93}Nb NMR spectroscopy, which, until recently, was only occasionally applied to niobium systems [4,5].

From the NMR point of view, solid-state ^{93}Nb NMR spectroscopy should be very effective in this regard, since the ^{93}Nb isotope ($I = 9/2$) is one of the most sensitive quadrupole nuclei (0.482 relative to ^{1}H) with a favorably

*Corresponding author. Fax: +7 383 330 80 56.
E-mail addresses: olga@catalysis.nsk.su, olga@catalysis.ru (O.B. Lapina).

0926-2040/$ - see front matter © 2005 Elsevier Inc. All rights reserved.
doi:10.1016/j.ssnmr.2005.09.003

low quadrupole moment ($-0.28 \times 10^{-28}\,m^2$). The second-order quadrupole broadening of the ^{93}Nb central transition should be only ca. 30% stronger than in ^{27}Al, assuming the same distortion. In practice, however, due to Sternheimer antishielding effects [5], ^{93}Nb NMR resonances tend to be much broader than for other quadrupole nuclei. As a result, ^{93}Nb is still relatively little studied nucleus. Solid-state ^{93}Nb NMR spectra of alkali metal niobates were investigated using static wide-line NMR spectroscopy [6–13]. Several niobates were studied using combined static and conventional MAS ^{93}Nb NMR [14–22].

In the last few years several advanced NMR techniques have been developed for quadrupole nuclei [23 and refs. therein], including ultrahigh speed magic angle spinning (UHS MAS), ultrahigh field experiments (UHF), double rotation (DOR) [24], dynamic-angle spinning (DAS) [25], multi-quantum magic angle spinning (MQMAS) [26], satellite transition spectroscopy (SATRAS, STMAS) [27,28], double-quantum satellite transition spectroscopy (DQ STMAS) [29], two-dimensional nutation [30], quadrupole phase-adjusted spinning sidebands (QPASS) [31], quadrupole echo Carr–Purcell–Meiboom–Gill magic angle spinning (QCPMG-MAS) [32]. At present, there is no universal method for quadrupole nuclei with a half-integer spin allowing one to obtain a complete set of quadrupole and chemical shielding (CS) tensor parameters for a wide range values of quadrupole constant and chemical shift anisotropy as observed in ^{93}Nb. Depending on the absolute values of these parameters and on their relative ratios certain NMR techniques or a combination of several NMR techniques should be applied. As it has been suggested in the literature, the most suitable for ^{93}Nb should be UHF and UHS experiments, solid-echo, MQMAS, pure-phase nutation, and STMAS [33–44].

Some of these techniques, in particular high-field MAS, MQMAS and quadrupole nutations, have been recently applied to ^{93}Nb NMR in lead niobates, polycrystalline $Pb(Mg_{1/3}Nb_{2/3})O_3$ and $Pb(Mg_{1/3}Nb_{2/3})O_3/PbTiO_3$ solid-solution ferroelectrics (PMN/PT) [33–38], and in niobium oxyfluorides [39,40]. In PMN/PT materials the detailed atomic-level structure of Nb(V) sites was obtained by ^{93}Nb MAS NMR combined with ^{93}Nb static nutation measurements. For octahedral $Nb(OMg)_6$ sites with cubic symmetry the isotropic ^{93}Nb chemical shift was found at -900 ppm (with respect to $NbCl_5$) and the quadrupole coupling constant $C_Q < 0.8$ MHz. The distortion of $Nb(ONb)_{6-x}(OMg)_x$ to tetragonal or rhombic symmetry had shown to dramatically increase the quadrupole coupling constant (to 17 and 62 MHz, respectively), and to shift isotropic lines up-field (to -954 and -980 ppm, respectively).

This last example with PMN/PT clearly demonstrates, that the modern solid-state ^{93}Nb NMR can be successfully applied to complex niobium-based systems. As only limited information on ^{93}Nb NMR in solid state is available to date, it is necessary to obtain ^{93}Nb NMR data for a wider range of individual niobium compounds, including those of practical importance, which can be found in various catalytic systems. Availability of such information may help in establishing possible correlations between the local structure of niobium sites and ^{93}Nb NMR parameters.

In this work, we have used conventional and UHF NMR facilities, UHS MAS, DQ STMAS, solid-echo and computer modeling to determine the CS and the quadrupole tensor parameters in a number of inorganic niobates with known crystalline structures. Based on these experimental results, as well as on the ^{93}Nb NMR data reported in the literature, the ^{93}Nb chemical shift scale for Nb–O compounds is introduced.

2. Experimental

2.1. NMR experiments

Solid-state ^{93}Nb NMR spectra were obtained at 97.77, 122.3 and 220.3 MHz (Bruker AVANCE-400, DSX-500 and ASX-900 spectrometers, respectively). Bruker 4.0 and 2.5 mm MAS probes were used for acquisition of static and 20–35 kHz MAS spectra. In single-pulse experiments the typical pulse width was 0.5 μs ($\pi/10$ "liquid-state"), the pulse delays varied from 0.3 to 1 s, and 12 000–200 000 transients were collected. The ^{93}Nb chemical shifts were referenced to an external saturated solution of $NbCl_5$ in acetonitrile.

Solid-echo spectra were measured according to [41]. The lineshape quality is of significant importance, since it should be compared to an ideal calculated spectrum. The quadrupole solid-echo sequence, $90°$–τ–$90°$, used in this work ($\tau = 100$ μs and effective $90°$ pulse 0.5 μs), is well adapted to record very broad static spectra, since it allows recording very short free induction decays without considerable distortions due to dead-time effects. Possible distortions were additionally minimized by a phase cycling proposed by Bodart [41].

Triple-quantum MAS (3Q MAS) experiments were performed using a basic three-pulse sequence with z-filter. The sequence begins with an excitation pulse $p1$ (1.4 μs) that creates 3Q coherence, which is allowed to evolve during the evolution period τ. A subsequent conversion pulse $p2$ (0.7 μs) flips magnetization back along the z-axis, which after a short (20 μs) delay (to allow dephasing of undesired coherences) is read out with a weak CT selective $90°$ pulse $p3$ (10 μs) [36].

Double-quantum satellite-transition MAS experiments (DQ STMAS) were executed with a shifted-echo mixing sequence. This pulse sequence effectively converts satellite-transition coherence from single- to double-quantum with a central-transition selective π-pulse. This conversion allows for selection of double-quantum coherence transfer pathways with phase cycling that filters out undesirable diagonal and outer satellite-transition peaks [29,42,43]. Experiments were performed on a Bruker ASX-900 spectrometer at 220.3 MHz using a 2.5 mm MAS probe. Pulses in the pulse sequence were defined as $p1$—excitation,

$p2$—central transition selective, $p3$—mixing, and $p4$—detection pulse. As a typical example, the parameters for the DQ STMAS experiment with $BiNbO_4$ were: $p1 = 1.2\,\mu s$, $p2 = 4\,\mu s$, $p3 = 0.5\,\mu s$, $p4 = 4\,\mu s$, initial $t_1 = 35.2\,\mu s$, $|\omega_1/2\pi| \sim 107\,kHz$ (for $p1$ and $p3$), $|\omega_1/2\pi| \sim 42\,kHz$ (for $p2$ and $p4$) with a recycle delay of 0.5 s for each of 32 t_1 increments. The z-filter delay τ_z and the shifted-echo delay τ were set at 4 and 3 ms, respectively. The first t_1 and 100 μs increment are synchronized with the 20 kHz MAS spinning rate. The 64-step phase cycle was used as described in [33–35]. The slope of double-quantum STMAS peaks is equal to that in a single-quantum STMAS plus one: for $I = 9/2$ this slope is 127/72. Since the slopes of QIS (13/8) and double-quantum (Aniso) (127/72) directions are very close, the value of the quadrupole constant could not be determined precisely. Nevertheless, the ^{93}Nb DQ STMAS experiments were useful when several non-equivalent Nb sites were present simultaneously in the sample. In such a case, the isotropic shifts were determined from the ^{93}Nb DQ STMAS, while the second-order corrections were performed with the quadrupole coupling constants estimated from the low-field static experiments.

Because ^{93}Nb MAS and static NMR spectra are often affected not only by quadrupole interactions but also by the CS interactions, a special approach has been developed based on a precise analysis of the spinning sidebands of the selected transitions [39,40]. This approach was used to determine the nuclear quadrupole coupling constant C_Q, the asymmetry parameter η_Q, and the isotropic chemical shift δ_{iso} in the presence of the large chemical shift anisotropy (Δ_δ) and the large quadrupole coupling constant (C_Q, η_Q, δ_{iso}, Δ_δ are defined in Table 1). The distances between the center band of the central transition and the spinning sidebands of the ($\pm 3/2 \leftrightarrow \pm 5/2$) satellite transition in the ^{93}Nb MAS NMR spectra are sensitive to the value of C_Q (^{93}Nb), while the line shapes are mainly determined by η_Q and the relative orientation of the quadrupole and CS tensors. The CS tensor can then be obtained by simulating the ^{93}Nb static NMR spectrum. Simulations of the MAS NMR spectra provided additional constraints on the fitting of all variable parameters. The ^{93}Nb MAS NMR spectra acquired at high and low magnetic fields and high and low MAS spinning speeds, as well as static spectra, were reproduced in the simulations. A more detailed description of this methodology will be given in Section 3. Simulations of the spectra were performed with the NMR5 software package developed by Shubin [44]. Two-dimensional spectra were analyzed with the DMFit simulation program [45].

2.2. Reagents and materials

Niobates were synthesized according to synthetic procedures published elsewhere [46–64]. The starting reagents (Li_2CO_3, Na_2CO_3, K_2CO_3, $CaCO_3$, Bi_2O_3, TeO_3, Y_2O_3, La_2O_3, SnO, $La(NO_3)_3$, $Pr(NO_3)_3$ and Nb_2O_5) with purity of 99% or higher were obtained from Aldrich.

Synthesis of alkali niobates and calcium niobate was performed by calcination in air corresponding alkali carbonates and Nb_2O_5 taken at a stoichiometric ratio. Thus, a three-step calcination was applied to synthesize Li_3NbO_4: for 5 h at 600 °C, then for 5 h at 850 °C, then for 12 h at 950 °C ($3Li_2CO_3 + Nb_2O_5 = 2Li_3NbO_4 + 3CO_2$).

Similarly, Na_5NbO_5 was obtained by calcination of $5Na_2CO_3 + Nb_2O_5 = 2Na_5NbO_5 + 5\,CO_2$ at 850 °C, 5 h, then at 900 °C, 5 h, then at 1000 °C, 12 h.

$KNbO_3$ ($2K_2CO_3 + Nb_2O_5 = 2KNbO_3 + 2CO_2$) was obtained by calcination at 870 °C, 5 h, then at 950 °C, 20 h.

$CaNb_2O_6$ ($CaCO_3 + N_2O_5 = CaNb_2O_6 + CO_2$) was obtained from a mixture of $CaCO_3$ and Nb_2O_5 prepared in acetone. This mixture was gradually heated to 1100 °C at a rate of 5 °C/min, kept at this temperature for 25 h and cooled to the room temperature at the same rate.

Bi_3NbO_7 ($3Bi_2O_3 + Nb_2O_5 = 2Bi_3NbO_7$) was synthesized from oxides by calcination at 800 °C, 10 h, then at 830 °C, 18 h.

$Te_3Nb_2O_{11}$ was also obtained from oxides ($3TeO_3 + Nb_2O_5 = Te_3Nb_2O_{11} + 1.5O_2$) by calcination at 700 °C, 8 h and 750 °C, 24 h.

$NaNb_3O_8$ was prepared from a precursor of the same composition by high-temperature calcination at high pressure: at 1100 °C, 30 kbar, 30 min.

$YNbO_4$, La_3NbO_7, $LaNb_5O_{14}$, α-$BiNbO_4$ samples were also prepared by air calcination of initial oxides under the following conditions: $YNbO_4$—1000–1250 °C, 30 h; La_3NbO_7—1000–1250 °C, 30 h; $LaNb_5O_{14}$—1000–1250 °C, 30 h; $BiNbO_4$—800, 5 h and 900 °C, 10 h.

Tin niobate $SnNb_2O_6$ was prepared as follows. Stoichiometric amounts of SnO and Nb_2O_5 were ground and thoroughly mixed in an agate mortar. This mixture was sealed in quartz ampoules under vacuum, calcined at 900 °C (heating rate 23 °C/min), kept at this temperature for 10 h, and cooled down with the same rate to the room temperature.

$MNbO_4$ (M = La, Pr) were obtained by a co-precipitation technique (from $NbCl_5$ and $M(NO_3)_3$ by NH_3) with subsequent calcination at 750–800 °C. This method allows one to lower the synthesis temperature by 400°C compared with the solid-state synthesis from oxides or hydroxides.

Calcination was performed in alundum crucibles. After each round of calcination the samples were thoroughly ground (or powdered) and pressed to form a tablet. Identification of synthesized compounds was confirmed with powder XRD (Siemens D-500 diffractometer, monochromatised CuK_α radiation) and HREM.

3. Results and discussion

3.1. NMR methodology used for ^{93}Nb NMR spectra analysis

^{93}Nb NMR spectra, even at very high magnetic fields, are dominated by the quadrupole interactions. The energy level diagram for ^{93}Nb ($I = 9/2$) and corresponding

Table 1
^{93}Nb quadrupole tensor parameters (C_Q, η_Q)[a], chemical shielding tensor parameters (η_δ, Δ_δ, δ_{iso})[b], and Euler angles (α, β, γ) describing relative orientation of the quadrupole tensor with respect to the chemical shielding tensor for individual niobium compounds

	C_Q (MHz)	η_Q	δ_{iso} (ppm)	η_δ	Δ_δ (ppm)	α	β	γ	Association of NbO_x polyhedra.	Methods	Ref.
					4-coordinated						
$YNbO_4$, monoclinic	81±2	0.41±0.05	−800±10	0	0	0		0	Isolated tetrahedra or oct. sharing 2 edges; $4O_t$, $2\mu_2$; 1.9522 × 2; 1.8359 × 2; 2.4 × 2 Å	Static	
	80	0.5	−750	0	0					HFMAS	
$LaNbO_4$, monoclinic	70±2	0.3±0.05	−650±25	0	0				Isolated tetrahedra or oct. sharing 2 edges; $4O_t$, $2\mu_2$; 1.844 × 2; 1.903 × 2; 2.53 × 2 Å	Static	
$PrNbO_4$, monoclinic	87±2	0.25±0.05	−400±100	0	0				Isolated tetrahedra or oct. sharing 2 edges; $4O_t$, $2\mu_2$	Static	
					5-coordinated						
Na_5NbO_5, monoclinic	11.1	0.01	−903	0	0				Isolated $5O_t$, 1.994 × 2, 1.900 × 2, 1.881	MAS	
	11.1	0.01	−903	0.6	120	0	31	90		HFMAS	
$CaNb_2O_6$, orthorhombic	50±2	0.8	−990	0.5	−300				Share 4 corners, $1O_t$, $3\mu_3$, $2\mu_2$;	Static	
	50	0.8	−990	0	−100				1.773–μ_2; 1.918–O_t; 1.947–μ_3; 2.064–μ_2; 2.077–μ_3; 2.342–μ_3	MAS	
					6-coordinated						
$Pb(Mg_{1/3}Nb_{2/3})_3$ cubic	<0.8		−900						Isolated octahedra $Nb(OMg)_6$	Nutation	[33]
Bi_3NbO_7, cubic	<20		−900						Share corners	MAS	
Li_3NbO_4, cubic	11.5	0.1	−950						Share 3 edges $3O_t$, $3\mu_2$ 1.858 × 3	MAS	
	12.0	0.1	−950	0.35	135				2.130 × 3	Static	
	12.0	0.1	−954	0.3	140					HFMAS	
α-$BiNbO_4$, orthorhombic	23	0.35	−963	0	0				Share 4 corners $2O_t$, $4\mu_2$	MAS	
	23	0.4	−963	0.25	−180				1.847 × 2 1.998 × 2 2.159 × 2	HFMAS	
	20.7	0.79	−974							3QMAS	
$Pb_3Nb_4O_{13}$, cubic	13.7±0.5		−995±5							3QMAS	[36]
$Pb(Mg_{1/3}Nb_{2/3})_3$ tetragonal	~17		−954 to −980						$Nb(ONb)_{6-x}(OMg)_x$	Nutation	[33]
$Pb(Mg_{1/3}Nb_{2/3})_3$ rhombic	>62		−954 to −980						$Nb(ONb)_{6-x}(OMg)_x$, $x = 1-5$	Nutation	[33]
La_3NbO_7, orthorombic	49	0.21	−980	0	0				Share 2 corners 1.936; 1.938 × 2,	Static	
	49	0.21	−980	0	0				2.035 × 2; 2.076	MAS	
$SnNb_2O_6$, monoclinic	38.7	0.67	−1010	0	0				Share 1 edge and 3 corners: $1O_t$, $3\mu_3$, $2\mu_2$ 1.848 μ_2; 1.873–O_t,	Static	
	40	0.45	−1010	0	0				1.976–μ_3; 2.035–μ_2 2.127–μ_3; 2.161–μ_3	MAS	
$LiNbO_3$, trigonal	22±0.5	0.01±0.05	−1004							Static	
	22.2	0.2	−996							MAS	
	22	0.2	−1004±4						Share 6 corners, 6 μ_2	MAS	[14]
	22.0	0	−1009						1.879 × 3	Single crystal	[8]
	22.1	—	−1004						2.125 × 3	3QMAS	[36]

Table 1 (*continued*)

	C_Q (MHz)	η_Q	δ_{iso} (ppm)	η_δ	Δ_δ (ppm)	α	β	γ	Association of NbO_x polyhedra.	Methods	Ref.
$NaNbO_3$, orthorhombic	22.7±0.5	—	−1073±5						Share 6 corners $6\mu_2$, 1.971×6	3QMAS	[36]
$KNbO_3$, orthorhombic	21.5	0.6	−1015		0				Share 6 corners $6\mu_2$, 1.874×2, 1.996×2, 2.168×2	MAS	
	23.1	0.80	−1069							HFMAS	[33]
$Sn_2Nb_2O_7$	<20		−1050±10						Share 6 corners	MAS	[19]
$PbNb_2O_6$, rhombic	16.8±0.5		−1113±5						Share edge and corners	3QMAS	[36]
	19±2	0.5±0.2	−1090±30	0.2±0.2	230±50	45±20	20±20	30±20		Single crystal	[34]
$Te_3Nb_2O_{11}$, orthorhombic	22	0.6	−1166	0	−150				Share 3 corners $3O_t$, $3\mu_2$	MAS	
	22	0.6	−1176	0.1	−250					HFMAS	
			−1207							STMAS	
$NbVO_5$	16.5	0.9	−1338±4						Share 2 corners,$4O_t$, $2\mu_2$	MAS	[14]
$Cdpy_4NbOF_5$ (py = C_5H_5N)	36.0(±0.5)	0.50(±0.05)	−1310	0.0	−666±20	0±20	0±2	0±20	Nonintersecting chains of alternating corner-sharing octahedra	HFMAS	[40]
$[pyH]_2[Cdpy_4\ (NbOF_5)_2]$	33.2(±0.5)	0.40(±0.05)	−1320	0.16	−700±20	60±20	5±2	0±20	Nonintersecting chains of alternating corner-sharing octahedra	HFMAS	[40]
6-coordinated with several Nb sites											
$Pb_2Nb_2O_7$, rhombic	13.6±0.5	9 sites	−1003±5							3QMAS	[36]
	17.0±0.5		−978±5								
$Pb_5Nb_4O_{15}$, rhombic	16.6±0.5	10 sites	−1013±5							3QMAS	[36]
	17.9±0.5		−975±5								
$Pb_3Nb_2O_8$, tetragonal	18.9±0.5	10 sites	−999±5							3QMAS	[36]
	20.6±0.5		−951±5								
7-coordinated											
$LaNb_5O_{14}$, orthorhombic	$Nb(1)O_6$		−1200						Nb(1) share edge Nb(1), 2 corners Nb(2), corner Nb(3); Nb(2) share edge Nb(3); Nb(3) share 2 edges and 2 corners Nb(2) and 2 corners Nb(1)	STMAS	
	$Nb(2)O_6$	3 sites	−1230								
	$Nb(3)O_7$		−1267								
K_2NbF_7 monoclinic	38.5	0.35	−1600	0	−200	45	0	0		HFMAS	[39]
8-coordinated											
$NaNb_3O_8$ orthorhombic									Share edges and corners:		
	$Nb(1)O_7$		−1250						Nb(1)–O: 1.834, 1.947, 1.948, 1.959, 2.212, 2.367×2	MAS	
	$Nb(2)O_8$		−1500						Nb(2)–O: 2.070×4, 2.081×4		

[a]Nuclear electric quadrupole moment eQ, electric field gradient tensor eigenvalues (V_{xx}, V_{yy}, and $V_{zz} = eq$) are connected with the quadrupole coupling constant C_Q and the asymmetry parameter η_Q by the relations: $C_Q = e^2qQ/h$; $V_{xx} = 1/2(-1 - \eta_Q)V_{zz}$; $V_{yy} = 1/2(-1+\eta_Q)V_{zz}$, where $|V_{zz}| \geqslant |V_{yy}| \geqslant |V_{xx}|$.

[b]The magnetic shielding is described by a second rank tensor with three components $\sigma_{ii}(i = 1, 2, 3)$ in its principal axis system, such that $|\sigma_{11} - \sigma_{iso}|$, $|\sigma_{22} - \sigma_{iso}| \leqslant |\sigma_{33} - \sigma_{iso}|$, where $\sigma_{iso} = (\sigma_{11} + \sigma_{22} + \sigma_{33})/3$. The chemical shift δ is related to the magnetic shielding according to the equation, $\delta_{ii} = (\sigma_{iso}(ref) - \sigma_{ii})/(1 - \sigma_{iso}(ref))$, where $\sigma_{iso}(ref)$– is the absolute isotropic magnetic shielding of the reference compound. The shielding tensor can be characterized by the following parameters: by the asymmetry parameter η_δ, the chemical shift anisotropy Δ_δ and the isotropic chemical shift δ_{iso} in the following manner: $\delta_{11} = 1/2\Delta_\delta\ (-1 - \eta_\delta) + \delta_{iso}$; $\delta_{22} = 1/2\Delta_\delta\ (-1 + \eta_\delta) + \delta_{iso}$; $\delta_{33} = \Delta_\delta + \delta_{iso}$. ($\alpha$, β, γ) Euler angles determining relative orientation of the chemical shielding and the quadrupolar tensors. When CS and quadrupole tensors coincide, (α, β, γ) are not shown. δ_{iso} was determined from the simulation of the spectra and presented here with the second-order quadrupole shift correction.

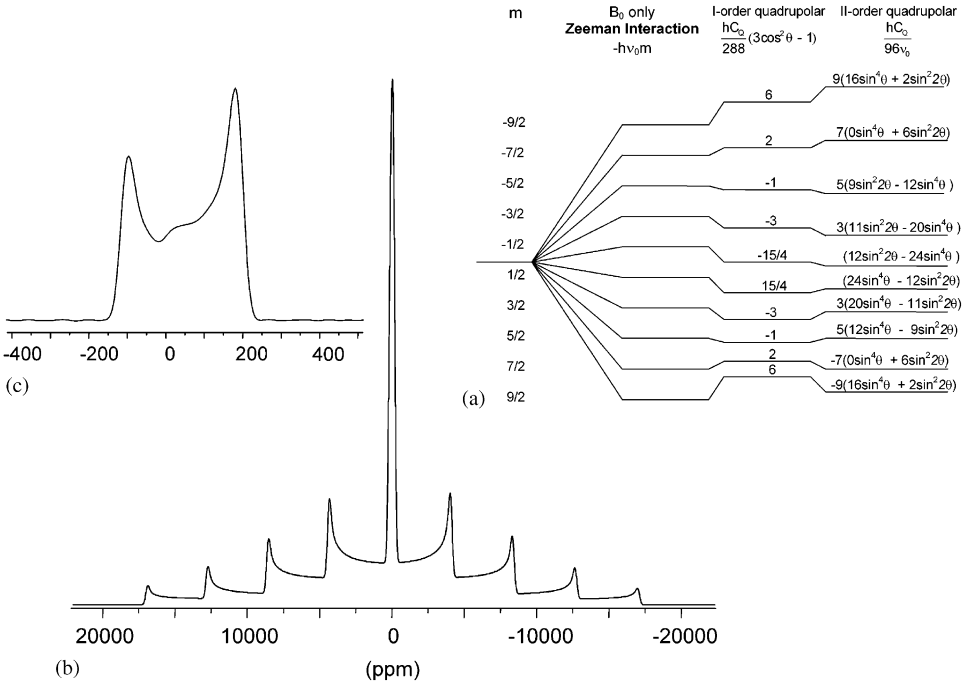

Fig. 1. Effects of the quadrupole interactions on the ^{93}Nb NMR spectra. (a) The energy-level diagram for $I = 9/2$. (b) Static spectrum due to the first-order quadrupole interactions. (c) Static spectrum (the central transition) due to the second-order quadrupole interactions. Simulation parameters: $C_Q = 20$ MHz, $\eta_Q = 0$, $\nu_0 = 97.9$ MHz.

theoretical spectra perturbed by the quadrupole interactions are shown in Fig. 1. For the central transition ($m_z = 1/2$), the dominant is the second-order quadrupole perturbation resulting in a characteristic powder pattern. Non-central transitions (i.e. $m_z \neq 1/2$) are spread wide from the central Larmor frequency. At the same time, for $I = 9/2$ nuclei, the satellite transitions are closer to the central transition compared with nuclei with lower spin quantum numbers (for a given C_Q). Thus, for $I = 9/2$ not only a central transition, but also several satellite transitions can be observed with conventional pulsed NMR spectrometers.

The magnitude of the quadrupole coupling constant in different Nb compounds can vary over a wide range, from hundreds of kHz to hundreds of MHz. For each individual compound, depending on the value of C_Q, the most appropriate NMR method was chosen. For the quadrupole constants less than 30 MHz, MAS, MQMAS, DAS, DOR, STMAS, and spinning sideband analysis of the selected transitions can be applied. The latter technique is the most convenient method for $I = 9/2$, and it was chosen in this work as the main research tool. The following iteration procedure was applied, which involved simultaneous analysis of MAS spinning sidebands and the static spectra:

As a first iteration step, an approximate value of the quadrupole constant was estimated from the low-field static spectra. This C_Q value was further rectified via spinning sideband analysis of the selected satellite transitions in MAS spectra. This method is based on the detailed analysis of the spinning sidebands of the satellite ($\pm 5/2 \leftrightarrow \pm 3/2$) and the central ($+1/2 \leftrightarrow -1/2$) transitions. According to Samoson et al. [24] in MAS spectra the shift $\delta^{(2)}$ and broadening $\Delta(m)$ caused by the second-order quadrupole interactions can be defined as

$$\delta^{(2)}(m) = \frac{3}{40}\frac{C_Q^2}{\nu_0^2}\frac{I(I+1) - 9m(m-1) - 3}{I^2(2I-1)^2}\left(1 + \frac{\eta^2}{3}\right), \quad (1)$$

$$\Delta(m) = \frac{3}{128}\frac{C_Q^2}{\nu_0^2}\frac{6I(I+1) - 34m(m-1) - 13}{I^2(2I-1)^2}\left(1 + \frac{\eta^2}{3}\right), \quad (2)$$

where I is the spin quantum number, $m = 1/2$ represents the central transition, $m = 3/2$ represents the satellite transition between $m = \pm 1/2$ and $\pm 3/2$, etc. Relative shifts of the satellite transitions with respect to the central transition for $I = 9/2$ were calculated by Grey et al. [39,40]. It was also concluded, that for $I = 9/2$ the $m = \pm 5/2$ satellite transition had the smallest broadening, 0.055 with respect to the central transition. As for the second order quadrupole shift, only for the $m = 3/2$ satellite transition does the quadrupole shift have the same sign as the central transition. These two effects are important in calculating quadrupole coupling constants from experimental ^{93}Nb MAS spectra.

Effects of C_Q on the spinning sidebands from satellite transitions at two magnetic fields are shown in Figs. 2 and 3. The range of quadrupole coupling constant that could be estimated from these satellite transitions is 15–50 MHz at 9.4 T and 20–80 MHz at 21.14 T. In experimental spectra the line shape of spinning sidebands will also depend on variations in η_Q [39,40]. Computer simulation of the full spectrum and the central transition

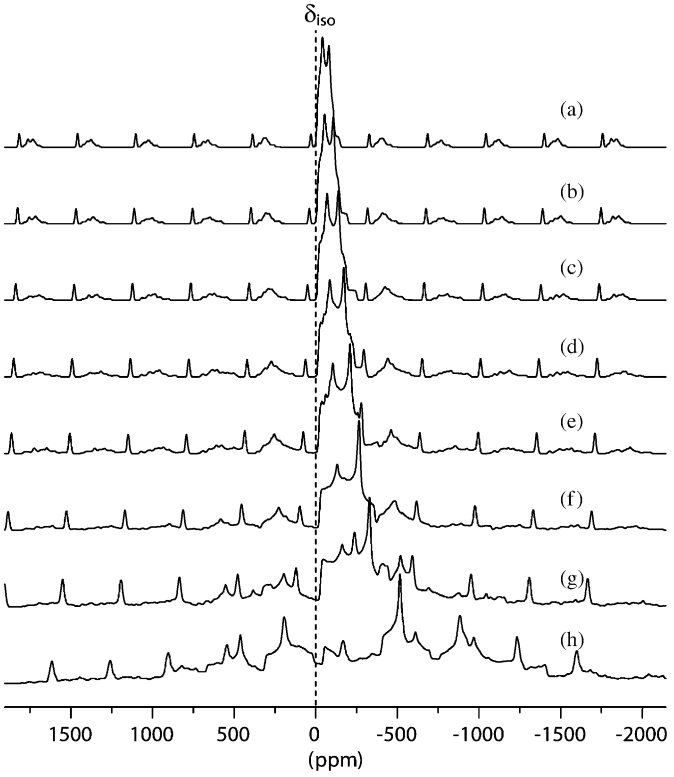

Fig. 2. Simulated ^{93}Nb MAS NMR spectra. Effects of the quadrupole coupling constant C_Q on the central transition ($\pm1/2 \leftrightarrow \pm1/2$) and the satellite transitions ($\pm3/2 \leftrightarrow \pm5/2$), ($\pm3/2 \leftrightarrow \pm1/2$). The simulation parameters: 9.4 T, $\eta_Q = 0.4$, $\delta_{iso} = 0$ ppm, $\nu_r = 35$ kHz, C_Q varies from 20, 23, 26, 29, 32, 36, 40 and 50 MHz spectra (a, b, c, d, e, f, g, h) respectively.

MAS spectra allows for accurate determination of C_Q, η_Q and δ_{iso} values (Fig. 4).

Using the values of C_Q, η_Q and δ_{iso} obtained from the analysis of satellites, it was possible to calculate chemical shift anisotropy parameters Δ_δ from analysis of the static

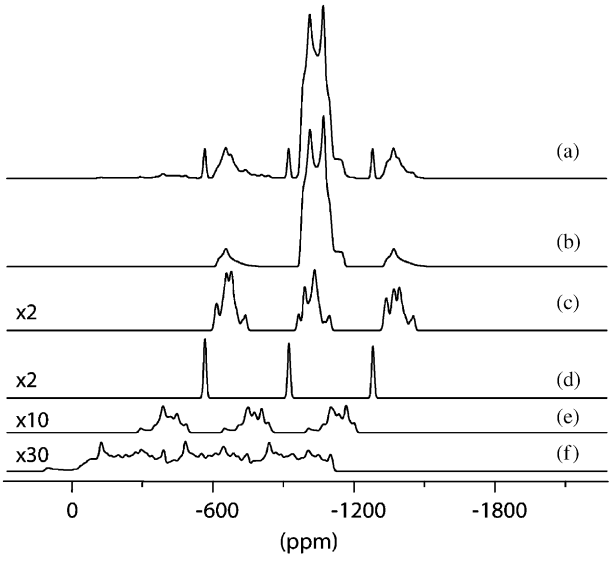

Fig. 4. Simulated ^{93}Nb MAS NMR spectra illustrating contributions from different transitions. (a) Spectrum including all transitions. (b) The central transition ($\pm1/2 \leftrightarrow \pm1/2$). The satellite transitions: (c) ($\pm3/2 \leftrightarrow \pm1/2$); (d) ($\pm5/2 \leftrightarrow \pm3/2$); (e) ($\pm7/2 \leftrightarrow \pm5/2$); (f) ($\pm9/2 \leftrightarrow \pm7/2$). Simulation parameters: $C_Q = 23$ MHz, $\eta_Q = 0.35$, $\delta_{iso} = -963$ ppm, $\nu_r = 30$ kHz.

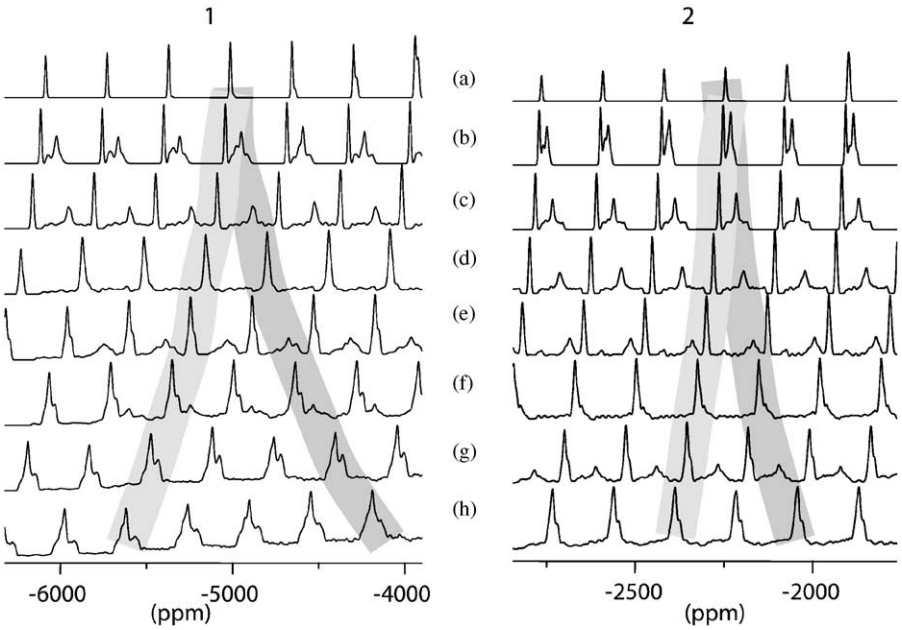

Fig. 3. Simulated ^{93}Nb MAS NMR spectra. Effects of the quadrupole coupling constant C_Q on the satellites transitions ($\pm3/2 \leftrightarrow \pm5/2$) and ($\pm3/2 \leftrightarrow \pm1/2$) at two different fields (1) 9.4 T, (2) 21.14 T. The simulation parameters: $\eta_Q = 0.4$, $\delta_{iso} = 0$ ppm, $\nu_r = 35$ kHz, C_Q varies from 10, 20, 30, 40, 50, 60, 70, 80 MHz spectra (a, b, c, d, e, f, g, h) respectively.

spectra recorded at different magnetic fields (at 97.77, 122.3 and 220.3 MHz). Static spectra recorded at higher fields are more informative in determination of CS tensor parameters, for example, at 21.14 T even small values of Δ_δ (~100 ppm) can be accurately calculated for compounds with C_Q~20 MHz.

The final set of CS and quadrupole tensor parameters for each compound was verified by comparing all experimental and once again simulated spectra (MAS and static) at different fields.

When the quadrupole coupling constant was higher than 50 MHz, the analysis of the spectra was done mainly for the low-field static spectra and the high-speed MAS spectra obtained at high field. However, in this case there were certain discrepancies between two sets of NMR parameters.

3QMAS and DQ STMAS NMR experiments were performed when several non-equivalent niobium sites were present in the structure simultaneously.

3.2. ^{93}Nb NMR spectra of individual niobates

The Nb coordination number in inorganic niobates varies from 4 to 8. The most typical are six-coordinated compounds. Not surprisingly, most of the ^{93}Nb NMR data reported so far are for six-coordinated Nb compounds, with an exception of K_2NbF_7, where the niobium coordination number is seven. Even for six-coordinated Nb only scarce information is available on the quadrupole coupling constants, CS tensors, the accurate isotropic shifts, orientations of CS and quadrupole tensors. There are no ^{93}Nb NMR data for four-, five- and eight-coordinated compounds. To fill this gap we have synthesized and analyzed with ^{93}Nb NMR a number of niobates with Nb in different coordination environments: four-coordinated ($LaNbO_4$, $YNbO_4$, $PrNbO_4$), five-coordinated (Na_5NbO_5, $CaNb_2O_6$), six-coordinated (Li_3NbO_4, Bi_3NbO_7, La_3NbO_7, $BiNbO_4$, $LiNbO_3$, $NaNbO_3$, $KNbO_3$, $SnNb_2O_6$, $Te_3Nb_2O_{11}$, $NbVO_5$), seven-coordinated ($LaNb_5O_{14}$, $NaNb_3O_8$) and eight-coordinated ($NaNb_3O_8$). These compounds have been selected because their crystalline structures are well known and available, e.g. in the Inorganic Crystal Structure Database (ICSD, ver. 2003).

3.2.1. Six-coordinated compounds

Li_3NbO_4: Li_3NbO_4 has cubic crystalline symmetry with space group *$I\bar{4}3m$*. The main structural elements of the body-centered cubic lattice are Nb_4O_{16} clusters consisting of four edge-sharing NbO_6 polyhedra [46,47]. Each NbO_6 shares three edges ($3O_t$, $3\mu_2$) with neighboring NbO_6 octahedra. Nb–O distances are reported as 1.858×3, 2.130×3 Å.

The ^{93}Nb NMR spectra for this compound are shown in Figs. 5–7. Because C_Q and the chemical shift anisotropy are not extremely large, it was possible to accurately calculate a full set of NMR parameters which fits well all the experimental spectra, including static, MAS, and HF-

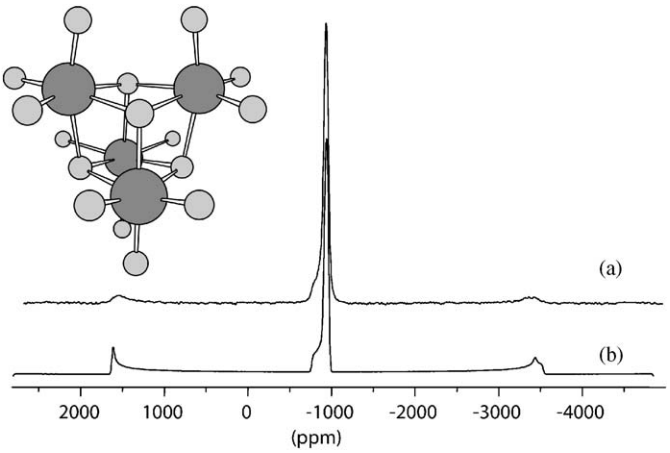

Fig. 5. (a) Experimental ^{93}Nb static spectrum of Li_3NbO_4 obtained with a quadrupole solid-echo sequence at 9.4 T. (b) Simulated ^{93}Nb static spectrum at 9.4 T with the following parameters: $C_Q = 12$ MHz, $\eta_Q = 0.1$, $\delta_{iso} = -950$ ppm, $\eta_\delta = 0.35$, $\Delta_\delta = 135$ ppm. The main structural unit in Li_3NbO_4 is a characteristic Nb_4O_{16} cluster consisting of four edge-sharing NbO_6 polyhedra as shown in the left upper corner.

MAS (Table 1). The ^{93}Nb static NMR spectrum recorded at 97.7 MHz has singularities of the first-order quadrupole perturbations (Fig. 5). Note that besides the central transition only the ($\pm 3/2 \leftrightarrow \pm 1/2$) transitions can be observed under these experimental conditions. C_Q estimated from the static spectrum is 12 MHz. In the ^{93}Nb MAS spectra at 9.4 T the satellite transitions for $m_z = 1/2$, 3/2, and 5/2 can also be seen (Fig. 6). Using spinning sidebands analysis as described above the accurate values of $C_Q = 11.5$ MHz and $\eta_Q = 0.1$ were obtained. The ^{93}Nb MAS NMR spectrum recorded at higher field had revealed moderate chemical shift anisotropy, $\Delta_\delta = 140$ ppm (Fig. 7). The isotropic chemical shift for Li_3NbO_4 was found at −950 ppm in all experiments.

α-$BiNbO_4$: α-$BiNbO_4$ has orthorhombic symmetry with centric space group *Pnna*. Both Bi and Nb have distorted octahedral oxygen coordination. NbO_6 octahedra are linked at four corners and the structure can be presented as flat sheets of $[NbO_4]^{3-}$ units separated by Bi^{3+} cations. The Nb–O distances are 1.847×2, 1.988×2, 2.159×2 Å ($2O_t$, $4\mu_2$) [48].

Analyzing distances between the center band of the central transition and spinning sidebands of the ($\pm 3/2 \leftrightarrow \pm 5/2$) satellite transitions at 9.4 T (Fig. 8), it was straightforward to find $C_Q = 23$ MHz, $\eta_Q = 0.35$ and the isotropic chemical shift at −963 ppm. High-speed MAS experiments at higher magnetic fields revealed the chemical shift anisotropy, Δ_δ, of −180 ppm. Because C_Q is not very large, NMR parameters were also calculated from the 3QMAS spectrum (Fig. 9). NMR parameters determined with different techniques were very close and well within the range of experimental errors (Table 1).

$LiNbO_3$: $LiNbO_3$ has rhombohedral symmetry with space group *R3c* and Nb–O distances at 1.876×3, 2.130×3 Å [49]. Anion (oxygen) and cation sublattices interpenetrate. Six equidistant O layers per *c*-axis are in an

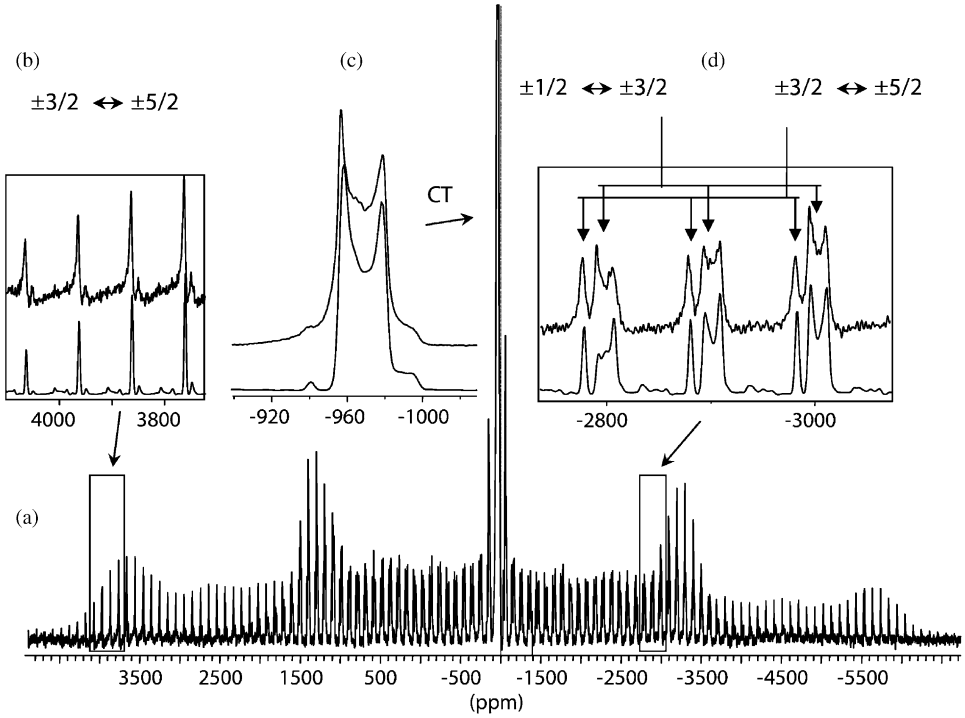

Fig. 6. (a) Experimental ^{93}Nb MAS spectrum of Li_3NbO_4 obtained at 9.4 T using a 4 mm MAS probe ($\nu_r = 10$ kHz). (b) The satellite transitions ($\pm 3/2 \leftrightarrow \pm 5/2$). (c) The central transition ($\pm 1/2 \leftrightarrow \pm 1/2$). (d) The satellite transitions ($\pm 3/2 \leftrightarrow \pm 1/2$) and ($\pm 3/2 \leftrightarrow \pm 5/2$). The lower spectra are simulated with parameters: $C_Q = 11.5$ MHz, $\eta_Q = 0.1$, $\delta_{iso} = -950$ ppm, $\nu_r = 10$ kHz.

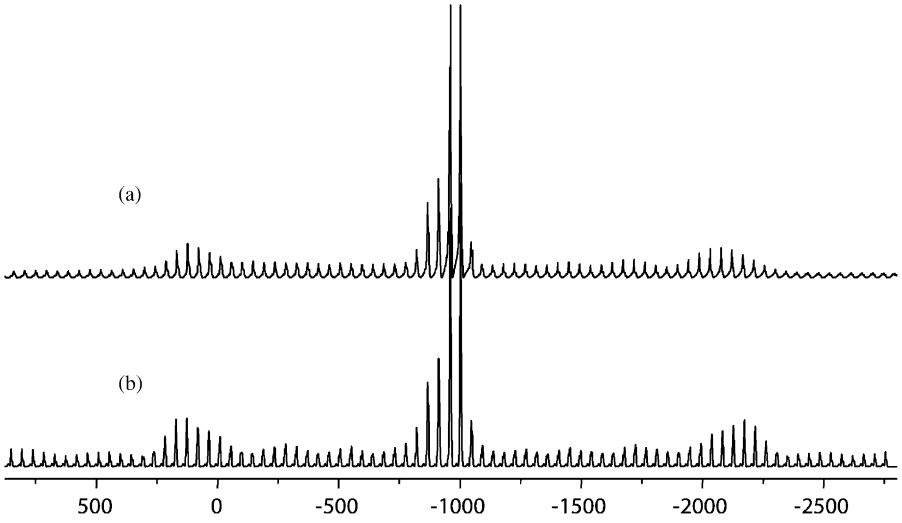

Fig. 7. (a) Experimental ^{93}Nb MAS spectrum of Li_3NbO_4 obtained at 21.14 T using a 2.5 mm MAS probe ($\nu_r = 9$ kHz). (b) Simulated ^{93}Nb MAS spectrum at 21.14 T with the following parameters: $C_Q = 12$ MHz, $\eta_Q = 0.1$, $\delta_{iso} = -954$ ppm, $\eta_\delta = 0.3$, $\Delta_\delta = 140$ ppm, $\nu_r = 9$ kHz.

anticlockwise–clockwise sequence with Nb-occupied, vacant and Li-occupied octahedral interstices. The cation sequence, Nb · vacancy · Li · Nb · vacancy · Li · Nb, is spaced non-uniformly along *c* and has one O layer in the second and fourth zones. Two O layers are interposed between Li…Nb atom pairs delineating the first and third zones. By analogy with the ideal ABO_3 perovskite structure, each Li atom has 12 O-atom neighbors. Three longest of the 12 Li–O vectors link to the O3 triangular face that is common to the NbO_6 and vacant O_6 octahedra. The remaining three Li–O vectors link to three O atoms coplanar with those linked by the shortest Li–O bonds.

Both the LiO_{12} and NbO_6 polyhedra are asymmetric. The Nb atom is 0.25 (4) [0.20 (4)] Å from the mid-point between the oxygen layers. The Li atom is 0.73 (1) [0.60 (2)] Å in the *c* direction from the double oxygen layers.

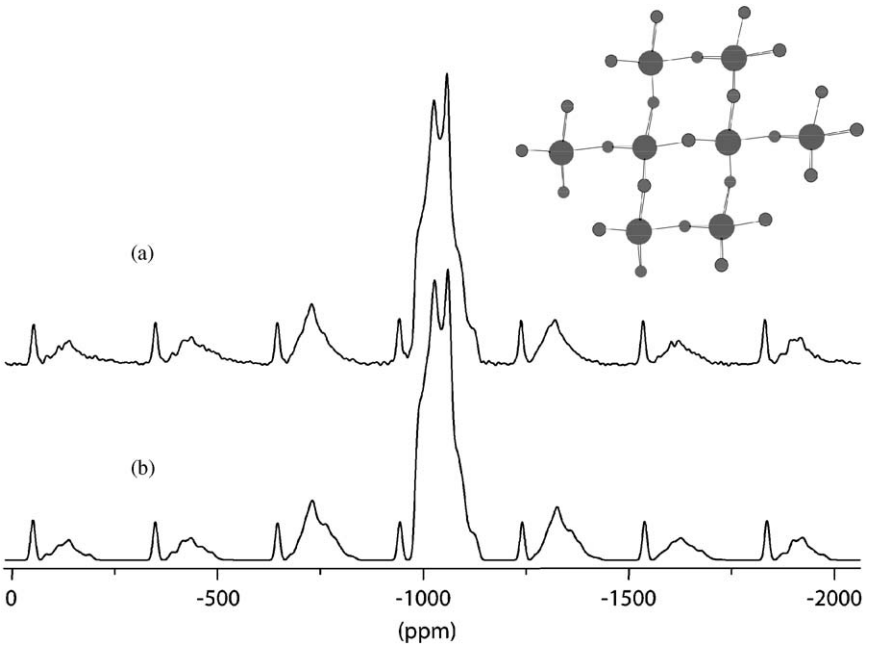

Fig. 8. (a) Experimental ^{93}Nb MAS spectrum of $BiNbO_4$ obtained at 9.4 T using a 2.5 mm MAS probe ($\nu_r = 30$ kHz). (b) Simulated ^{93}Nb MAS spectrum at 9.4 T with the following parameters: $C_Q = 23$ MHz, $\eta_Q = 0.35$, $\delta_{iso} = -963$ ppm. Structure of $BiNbO_4$ is formed by corner-linked NbO_6 octahedra forming flat sheets of $[NbO_4]^{3-}$ units separated by Bi^{3+} cations (a fragment of the sheet is shown in the right corner).

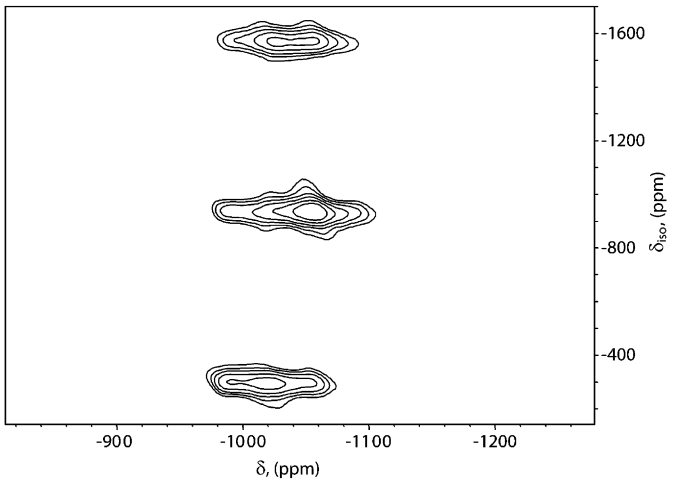

Fig. 9. Experimental ^{93}Nb 3QMAS NMR spectrum of $BiNbO_4$ obtained at 9.4 T. $C_Q = 20.7$ MHz, $\eta_Q = 0.79$, $\delta_{iso} = -974$ ppm.

Displacive Δz vectors for Li and Nb nuclei defined in this manner are parallel.

$LiNbO_3$ is the only niobium compound thoroughly investigated with solid-state ^{93}Nb NMR [5–12]. As a matter of fact, all the new NMR techniques applicable to $I = 9/2$ have been first tested on $LiNbO_3$ [36,41,42,50]. Regardless of different resources of these NMR studies, the NMR parameters obtained were similar. We have also tested our approach with $LiNbO_3$. NMR parameters obtained for $LiNbO_3$ from ^{93}Nb static (not shown) and MAS NMR (Fig. 10) spectra are summarized in Table 1. These parameters are in close agreement with previously reported.

$KNbO_3$: $KNbO_3$ At room temperature $KNbO_3$ exists in orthorhombic phase, space group *Amm2*, NbO_6 shares all six corners with neighboring NbO_6 ($6\mu_2$). Nb–O distances are 1.874×2, 1.996×2, 2.168×2 Å [51,52].

Structures of alkali (Li, Na, K) niobates are similar [49–53], the same is also true for their corresponding ^{93}Nb NMR spectra. The ^{93}Nb MAS spectrum of $KNbO_3$ is shown in Fig. 11. This spectrum is very similar to $LiNbO_3$, even though, due to a larger value of $\eta_Q = 0.6$, the line shape is not as defined as in $LiNbO_3$. It is interesting that the ferroelectric behavior of $LiNbO_3$ has been directly connected to this asymmetry parameter ($\eta_Q \sim 0.01$ in $LiNbO_3$). It was suggested that in $LiNbO_3$ the macroscopic electric dipole moment is parallel to the *c*-axis, which is perpendicular to the planes of oxygen atoms. This coincidence has been attributed to near axial symmetry in the perovskite structure [8–11,49].

$SnNb_2O_6$: $SnNb_2O_6$ has monoclinic space group *C12/c1* with Nb–O distances at 1.848, 1.873, 1.976, 2.035, 2.127, 2.161 Å (O_t, $2\mu_2$, $3\mu_3$). The structure represents two types of alternating layers perpendicular to the *x*-axis. One type of layers consists of corner-linked NbO_6 octahedra forming flat perforated two-octahedron-thick sheets with closest-packed anions. The other layer consists of distorted edge-sharing SnO_8 square antiprisms [54]. ^{93}Nb static and MAS NMR spectra for this compound are characterized by a very large quadrupole coupling constant (~40 MHz) and $\eta_Q \sim 0.5$. At the same time the isotropic chemical shift found in this compound (−1010 ppm) is similar to alkali niobates (Table 1). As in the previous cases, the NMR parameters were obtained from both static and MAS spectra (Figs. 12

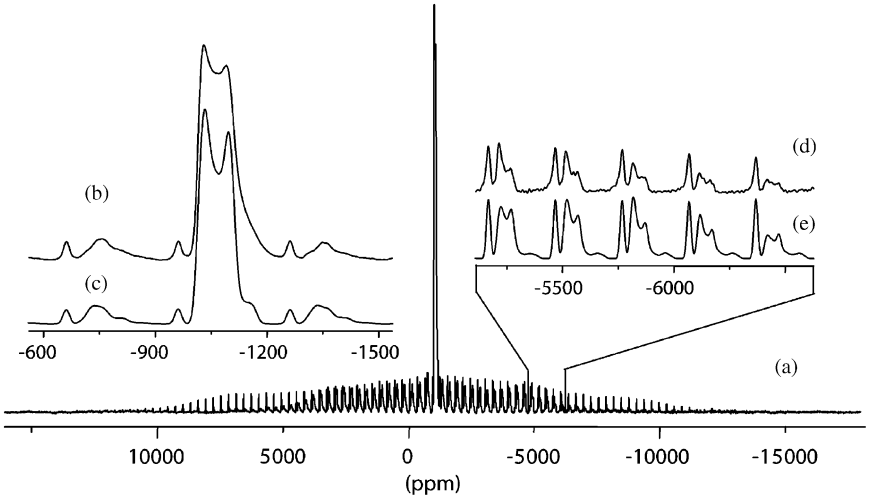

Fig. 10. (a) Experimental ^{93}Nb MAS spectra of $LiNbO_3$ obtained at 9.4 T using a 2.5 mm MAS probe ($\nu_r = 30$ kHz). (b) The satellites transitions ($\pm 3/2 \leftrightarrow \pm 1/2$), and the central transition ($\pm 1/2 \leftrightarrow \pm 1/2$). (d) The satellites transitions ($\pm 3/2 \leftrightarrow \pm 1/2$) and ($\pm 5/2 \leftrightarrow \pm 3/2$). (c and e) Simulated spectra with parameters: $C_Q = 22$. MHz, $\eta_Q = 0.2$, $\delta_{iso} = -996$ ppm, $\nu_r = 30$ kHz.

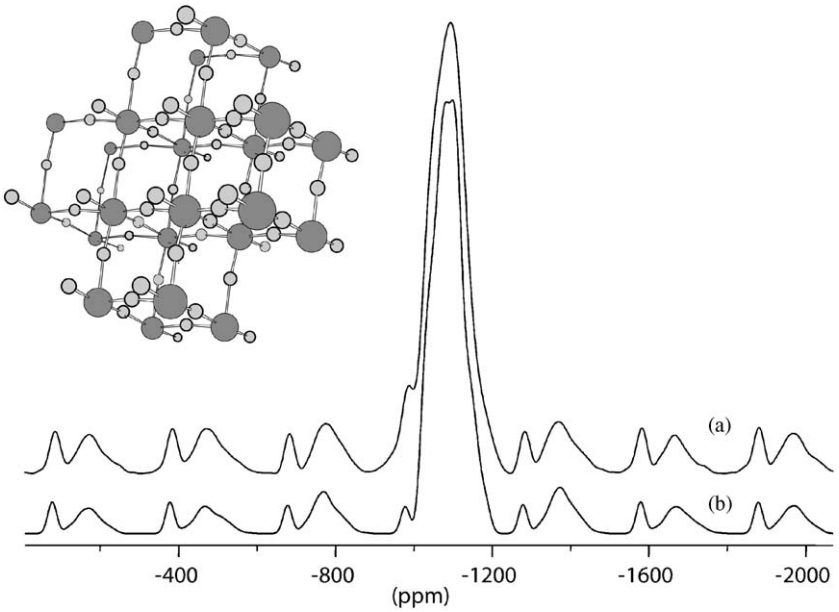

Fig. 11. (a) Experimental ^{93}Nb MAS spectrum of $KNbO_3$ obtained at 9.4 T using a 2.5 mm MAS probe ($\nu_r = 30$ kHz). (b) Simulated ^{93}Nb MAS spectrum at 9.4 T with the following parameters: $C_Q = 21.5$ MHz, $\eta_Q = 0.6$, $\delta_{iso} = -1015$ ppm, $\nu_r = 30$ kHz. $KNbO_3$ exists in orthorhombic phase, each NbO_6 shares six corners with neighboring NbO_6 (fragment is shown in the left corner).

and 13). The MAS spectra were analyzed using separation between the center band of the central transition and sidebands of the ($\pm 3/2 \leftrightarrow \pm 5/2$) satellite transitions at 9.4 T.

La_3NbO_7: La_3NbO_7 The unit cell of La_3NbO_7 is orthorhombic, with centrosymmetric space group *Pnma*. Stacking of NbO_6 octahedra is described in terms of zig-zag chains aligned along the *a*-axis of the crystal. Lanthanum ions occupy two different sites with coordination polyhedra consisting of seven or eight oxygen neighbors, and Nb atoms are off-center in their corresponding octahedra, so that the Nb–O distances are found at 1.936, 1.938 × 2, 2.035 × 2, 2.076 Å [55].

It seems that the niobium coordination in zig-zag chains of NbO_6 octahedra is very close to symmetric. Nevertheless, due to the fact that Nb atoms are off-center, the observed ^{93}Nb NMR line is broad (Fig. 14) and the quadrupole coupling constant is almost 50 MHz with the symmetry of the quadrupole tensor close to axial ($\eta_Q = 0.2$). The isotropic shift (−980 ppm) is smaller than in alkali niobates.

$Te_3Nb_2O_{11}$: $Te_3Nb_2O_{11}$ has an orthorhombic unit cell with space group *$P2_12_12$*. Infinite corner-sharing pairs of NbO_6 octahedra are connected via finite >Te–O–Te–O–Te< strings forming a three-dimensional net. Three-coordinated

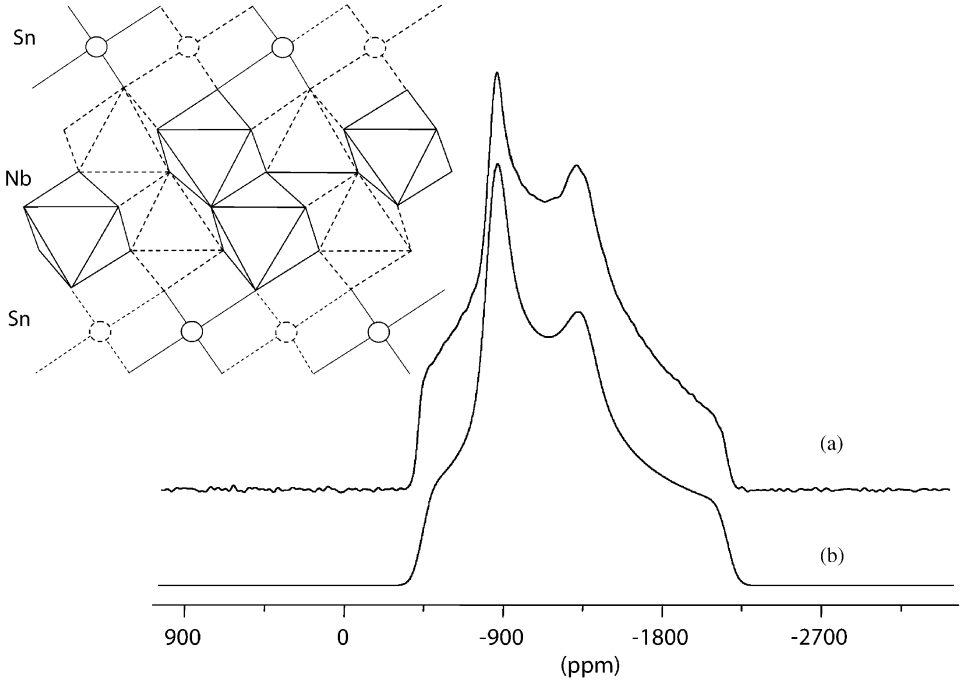

Fig. 12. (a) Experimental ^{93}Nb static spectrum of $SnNb_2O_6$ obtained with a quadrupole solid-echo sequence at 9.4 T. (b) Simulated ^{93}Nb static spectrum at 9.4 T with the following parameters: $C_Q = 40$ MHz, $\eta_Q = 0.1$, $\delta_{iso} = -1010$ ppm, $\eta_\delta = 0$, $\Delta_\delta = 0$ ppm. Structure of $SnNb_2O_6$ consists of two alternating layers. One layer of corner-linked NbO_6 octahedra forms a flat perforated two-octahedron-thick sheet with closest-packed anions. The other layer consists of distorted edge-sharing SnO_8 square antiprisms (shown in the left upper corner).

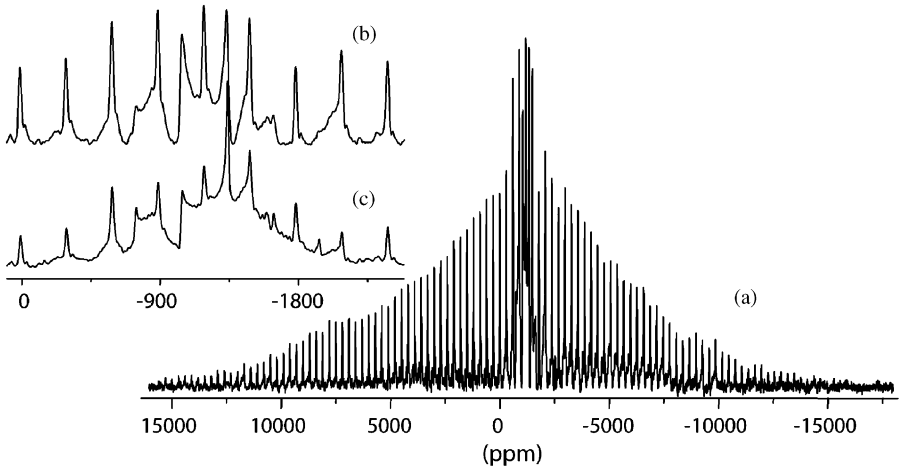

Fig. 13. (a) Experimental ^{93}Nb MAS spectrum of $SnNb_2O_6$ obtained at 9.4 T using a 2.5 mm MAS probe ($\nu_r = 35$ kHz). (b) The central part of the experimental spectrum. (c) Simulated ^{93}Nb MAS spectrum with parameters: $C_Q = 40$ MHz, $\eta_Q = 0.45$, $\delta_{iso} = -1010$ ppm, $\eta_\delta = 0$, $\Delta_\delta = 0$ ppm, $\nu_r = 35$ kHz.

Te(IV) atoms have normal pyramidal configuration (Te–O = 1.84, 1.86 and 1.86 Å), while four-coordinated Te(IV) atoms have unusual configuration within a tetrahedron of oxygen atoms. The average Nb–O bond distance of 2.00 Å is considered normal. However, Nb atoms are displaced from the center of oxygen octahedrons along the polar axis (chain direction), to give alternating, short and long, Nb–O distances of 1.80 and 2.19 Å [56]. This off-center displacement of Nb atoms results in C_Q value of ~22 MHz, and in the asymmetry parameter $\eta_Q = 0.6$. It is important that Δ_δ also reflects the asymmetric character of niobium surrounding in this compound. Δ_δ value can be found from the high-field NMR experiments, and it is close to −250 ppm (see Figs. 15 and 16, and Table 1), the isotropic chemical shift $\delta_{iso} \sim -1190$ ppm.

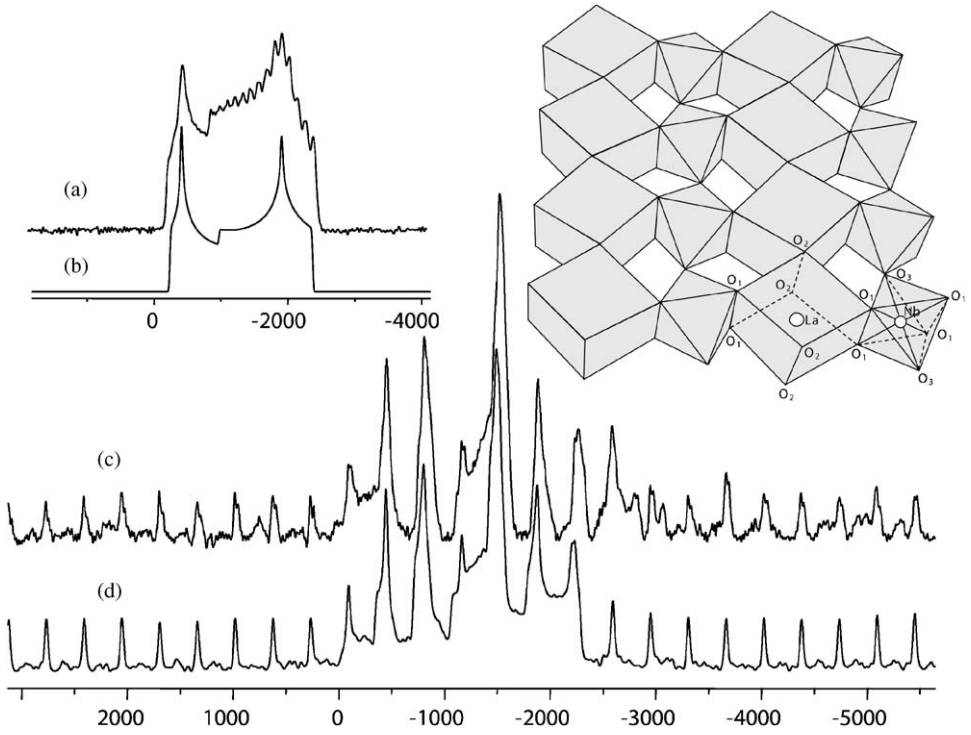

Fig. 14. (a) Experimental ^{93}Nb static and (c) MAS spectra of La_3NbO_7 obtained at 9.4 T using 4 and 2.5 mm MAS probes, respectively. (b) Simulated ^{93}Nb static and (d) MAS spectra. Parameters used in a simulation: $C_Q = 49$ MHz, $\eta_Q = 0.21$, $\delta_{iso} = -980$ ppm, $\eta_\delta = 0$, $\Delta_\delta = 0$ ppm, $\nu_r = 35$ kHz. Structure of La_3NbO_7 comprises zig-zag chains of NbO_6 octahedra. Lanthanum ions occupy two different polyhedra (shown in the right upper corner).

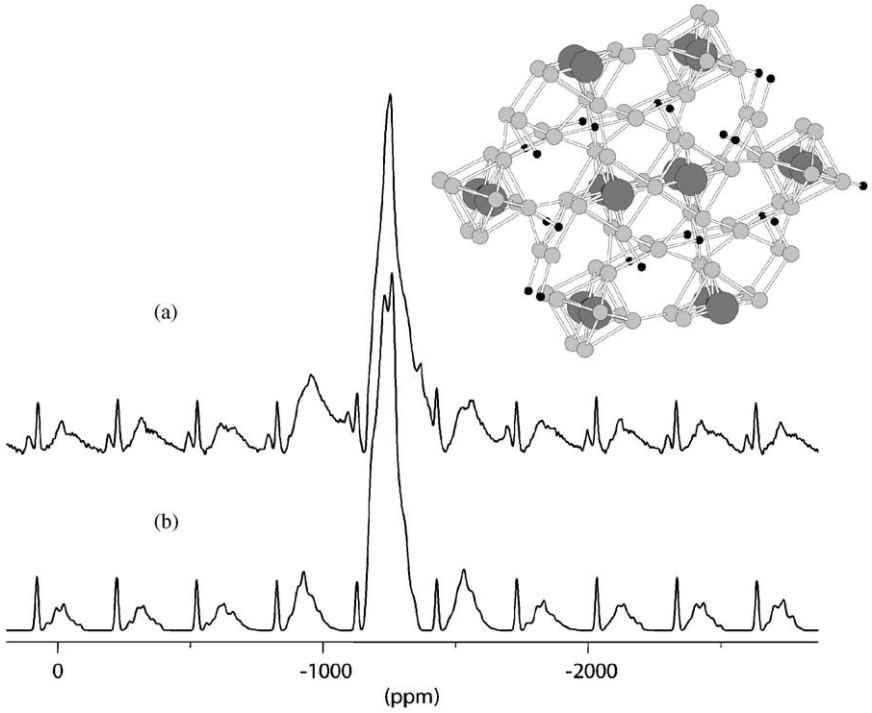

Fig. 15. (a) Experimental ^{93}Nb MAS spectrum of $Te_3Nb_2O_{11}$ obtained at 9.4 T using a 2.5 mm MAS probe ($\nu_r = 30$ kHz). (b) Simulated ^{93}Nb MAS spectrum with the following parameters: $C_Q = 22$ MHz, $\eta_Q = 0.6$, $\delta_{iso} = -1166$ ppm, $\eta_\delta = 0$, $\Delta_\delta = 150$ ppm, $\nu_r = 30$ kHz. The structure of $Te_3Nb_2O_{11}$ includes infinite pairs of corner-sharing NbO_6 octahedra connected via finite >Te–O–Te–O–Te< strings, thus forming a three-dimensional net (shown in the right corner).

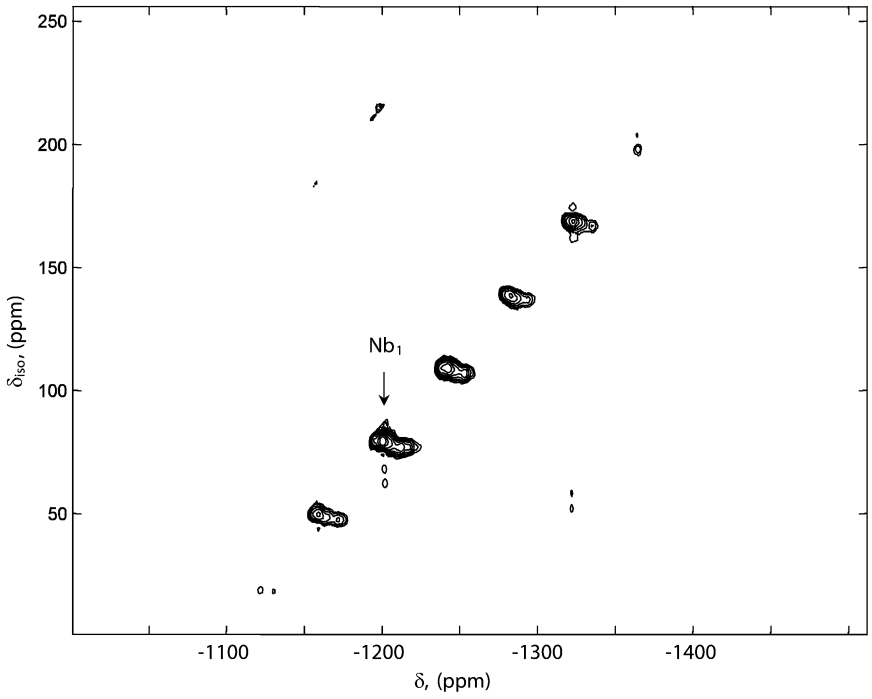

Fig. 16. ^{93}Nb DQ STMAS spectrum of $Te_3Nb_2O_{11}$ obtained at 21.14 T ($\nu_r = 20$ kHz).

3.2.2. NMR features typical for six-coordinated Nb sites

^{93}Nb NMR parameters for six-coordinated Nb sites for different niobium compounds as determined in this work and reported in the literature are summarized in Table 1. Based on these data the following common features for NbO_6 sites can be identified:

(1) the isotropic chemical shift δ_{iso} for Nb in octahedral sites occurs from −900 to −1300 ppm;
(2) for sites with cubic symmetry the typical δ_{iso} range is −900 to −1000 ppm;
(3) for sites with non-cubic symmetry, the isotropic chemical shifts seem to depend on the ionic character of the niobium sublattice: (i) in niobates of M (+1, +2, +3) elements the niobium sublattice has more anionic character, and the isotropic shifts are in the range from −1000 to −1100 ppm; (ii) when M(+4) or M(+5) is present, the niobium sublattice has more covalent (towards cationic) character and the isotropic chemical shifts are shifted to −1200 to −1300 ppm;
(4) the quadrupole coupling constant depends on the site symmetry and not on the coordination number, C_Q can vary in a wide range, from hundreds of kHz to hundreds of MHz;
(5) the chemical shift anisotropy is more pronounced when different atoms are present in the first coordination sphere, e.g. O and F.

Previously [14], the high-field ^{93}Nb isotropic shifts in $NbVO_5$ compared to $LiNbO_3$ were explained by a better shielding of ^{93}Nb nuclei in $NbVO_5$, where Nb octahedra are sharing corners, while in $LiNbO_3$ Nb octahedra are sharing edges. Exactly the opposite explanation of the shielding effects was given for lead niobates [36]. Thus, the unusual high-field ^{93}Nb shift in $PbNb_2O_6$ (−1156 ppm) was attributed to its unique structure, which consists of both edge- and corner-sharing NbO_6 octahedra, while other lead niobates has only corner-sharing NbO_6 octahedra in their structures [36]. From the data presented in Table 1, it becomes clear that no obvious correlation exists between the isotropic shift value and the way of sharing of NbO_6 octahedra. Thus, the isotropic shift could be very small or very large for the same type of corner-sharing structures. At the same time, for sites with non-cubic symmetry, the ^{93}Nb isotropic chemical shifts seem to depend on the ionic character of the niobium sublattice in NbO_x–MO_y. In other words, the shift in position of the ^{93}Nb isotropic chemical shift may reflect the gradual transformation of the Nb sublattice in niobates from anionic to cationic depending on the type of counter-ions, M (+1, +2, +3) vs. M (+4, +5).

3.3. Four-coordinated compounds

$MNbO_4$ (M = Y, La, Pr): $YNbO_4$ has monoclinic symmetry with space group *C12/c1*. NbO_4 tetrahedra in $YNbO_4$ are strongly distorted with Nb–O distances 1.9522×2 and 1.8359×2 Å (Fig. 17) [57]. Neighboring NbO_4 tetrahedra are in close proximity, with distances from niobium to neighboring oxygen atoms about 2.4–2.5 Å. For this reason, NbO_x polyhedra in $YNbO_4$ are often considered as intermediate between isolated NbO_4 tetrahedra and edge-sharing chains of NbO_6 octahedra with two long Nb–O bonds [57–59]. It may be

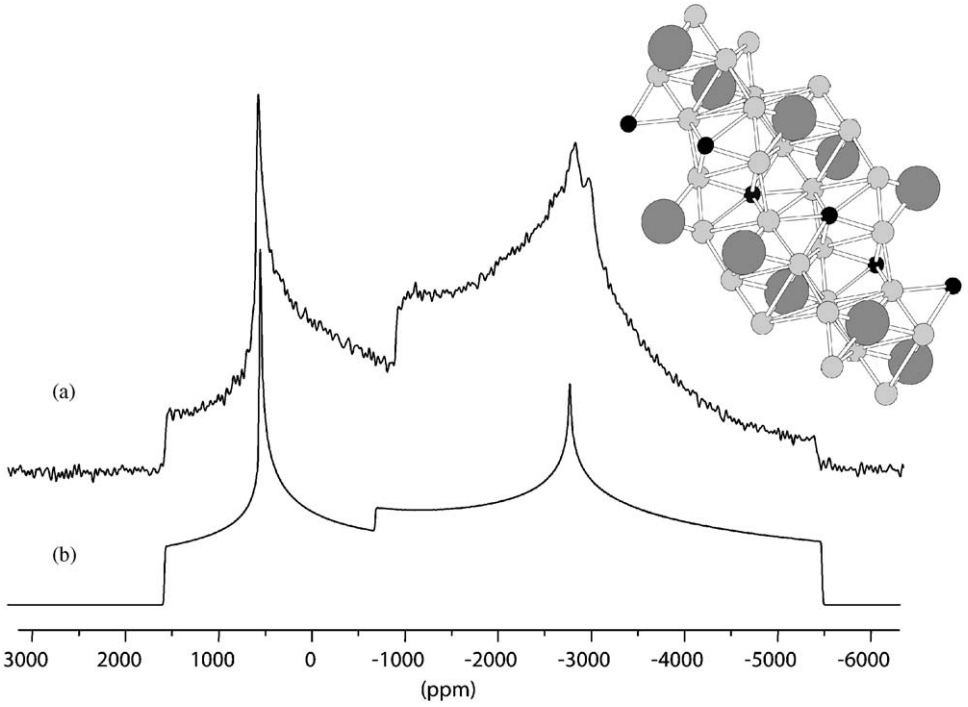

Fig. 17. (a) Experimental ^{93}Nb static spectrum of $YNbO_4$ obtained with a quadrupole solid-echo sequence at 9.4 T. (b) Simulated ^{93}Nb static spectrum at 9.4 T with the following parameters: $C_Q = 81$ MHz, $\eta_Q = 0.4$, $\delta_{iso} = -800$ ppm, $\eta_\delta = 0$, $\Delta_\delta = 0$ ppm. The crystalline structure of $YNbO_4$ is shown in the right upper corner. NbO_4 tetrahedra are strongly distorted and are in close proximity. Nb–O distances between neighboring tetrahedra are short enough (2.4–2.5 A), to consider Nb–O polyhedra as intermediate between isolated NbO_4 tetrahedra and edge sharing chains of NbO_6 octahedra with two long Nb–O bonds.

possible to answer with ^{93}Nb NMR spectroscopy which of the structures is more adequate.

^{93}Nb NMR spectra of $YNbO_4$ differ significantly from the spectra of compounds with well-defined NbO_6 octahedra in their structure. The ^{93}Nb NMR static spectrum of $YNbO_4$ is very broad, and it was practically impossible to record this spectrum without distortions (Fig. 17) [41]. Computer simulation of this spectrum has produced a very large quadrupole coupling constant (80 MHz) and the isotropic shift shifted unusually to −800 ppm. Similar parameters were also found for $LaNbO_4$ ($C_Q = 70$ MHz, $\delta_{iso} = -650$ ppm, Table 1).

UH MAS and DQ STMAS NMR experiments (Fig. 18) did not improve the situation, with discrepancies still remaining between NMR parameters determined from static and MAS spectra (Table 1). It is possible to conclude, however, that the NMR parameters obtained for $YNbO_4$ and $LaNbO_4$ are quite different from those for octahedral Nb sites, and the most characteristic feature is the value of isotropic shift (see Table 1).

Crystalline structures of $MNbO_4$ (M = RE—Rare Earth elements) are very similar. Unfortunately, almost all these compounds are paramagnetic, which complicates their ^{93}Nb NMR studies. When paramagnetic effects are not as strong, e.g. for Pr, it was possible to obtain ^{93}Nb NMR spectra and to calculate corresponding NMR parameters (Table 1). The ^{93}Nb isotropic chemical shift in $PrNbO_4$ differs considerably from $YNbO_4$ and $LaNbO_4$, most likely due to paramagnetic effects.

Thus, the ^{93}Nb isotropic chemical shifts for four-coordinated Nb sites occur in the lower field range (−400 to −900 ppm) compared with six-coordinated Nb sites. Due to significant distortion of the local environment in four-coordinated sites and their pseudo-octahedral type, the quadrupole coupling constants are usually very large >70 MHz.

3.4. Five-coordinated compounds

Na_5NbO_5: Na_5NbO_5 has monoclinic symmetry and space group *C2/c*. The NaCl-type crystal structure is created by ordering cations and oxygen vacancies in the anionic sublattice. The corresponding structural formula is best described as $Na_{5/6}Nb_{1/6}O_{5/6}\square_{1/6}$. Sodium and niobium atoms have distorted square–pyramidal oxygen surroundings. Niobium pyramids are isolated. Niobium–oxygen distances are found at 1.994 × 2, 1.900 × 2, 1.881 Å [60].

^{93}Nb NMR spectra for Na_5NbO_5 are different from the spectra of four-coordinated Nb compounds by a much smaller quadrupole coupling constant (11 MHz) and by a significant high-field shift of δ_{iso}. The complete set of NMR parameters for this compound was determined from NMR experiments at different magnetic fields (Figs. 19 and 20,

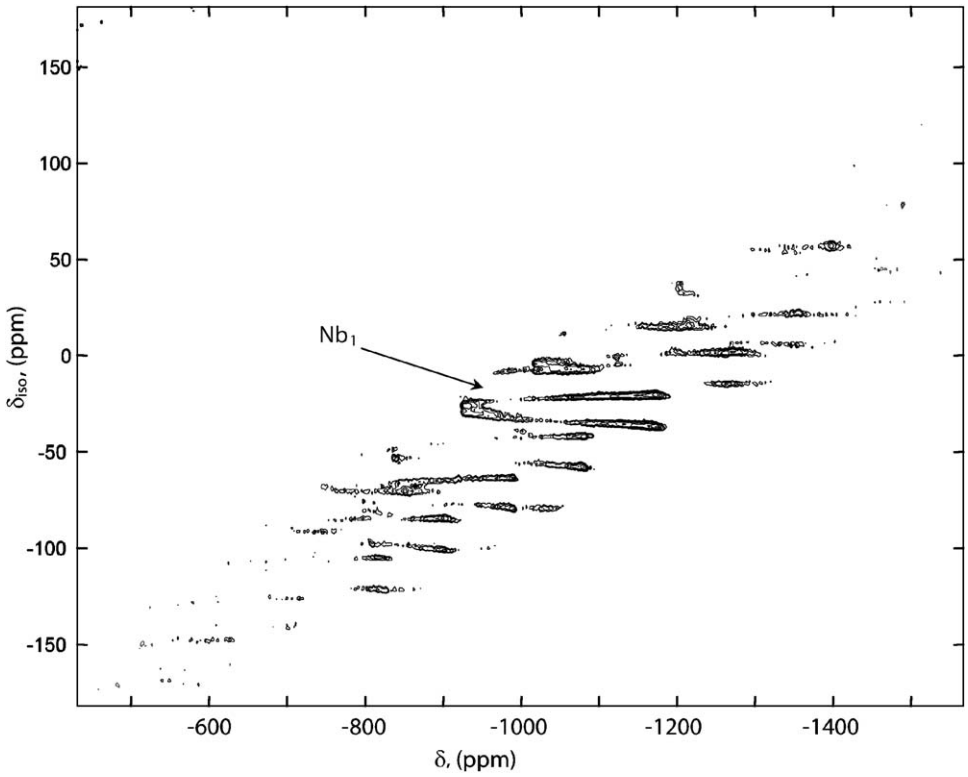

Fig. 18. ^{93}Nb DQ STMAS spectrum of $YNbO_4$ obtained at 21.14 T ($\nu_r = 20$ kHz).

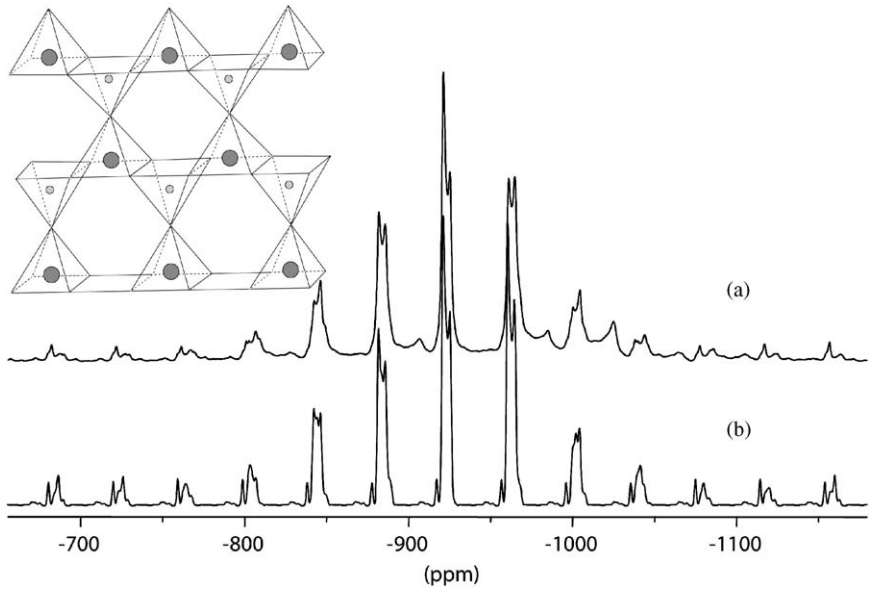

Fig. 19. (a) Experimental ^{93}Nb MAS spectrum of Na_5NbO_5 obtained at 21.14 T using a 2.5 mm MAS probe ($\nu_r = 8$ kHz). (b) Simulated ^{93}Nb MAS spectrum with the following parameters: $C_Q = 11.1$ MHz, $\eta_Q = 0.01$, $\delta_{iso} = -903$ ppm, $\eta_\delta = 0.6$, $\Delta_\delta = -120$ ppm, $\nu_r = 8$ kHz. The structure of Na_5NbO_5 includes isolated sodium and niobium square–pyramids as shown in the left corner.

Table 1). The CS tensor parameters and tensors orientation were obtained only from high-field measurements. The small value of the quadrupole constant reflects the symmetric nature of Nb sites and their isolated character. The high-field shift as compared with four-coordinated compounds is due to higher coordination number.

$CaNb_2O_6$: $CaNb_2O_6$ has orthorhombic symmetry, space group *Pbcn*. Nb–O distances are 1.773, 1.918, 1.947, 2.064, 2.077, 2.342 Å ($1O_t$, $3\mu_3$, $2\mu_2$). Each niobium octahedron shares two edges with adjacent niobium octahedra, thus forming chains of octahedra. Niobium octahedra are linked to each other along their shortest edges. Chains

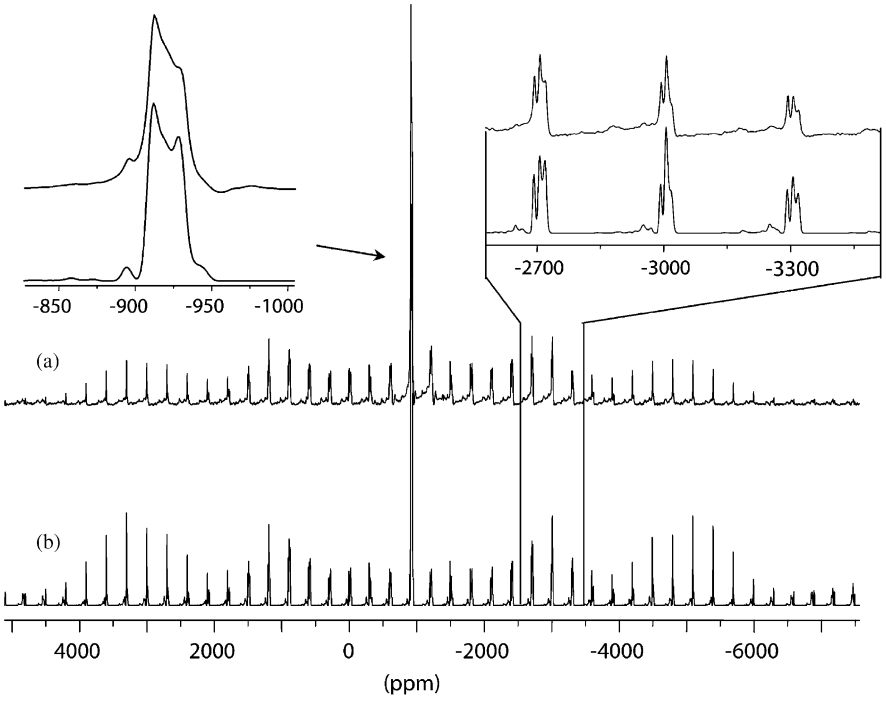

Fig. 20. (a) Experimental ^{93}Nb MAS spectrum of Na_5NbO_5 obtained at 9.4 T using a 2.5 mm MAS probe ($\nu_r = 30$ kHz). (b) Simulated ^{93}Nb static spectrum with the following parameters: $C_Q = 11.1$ MHz, $\eta_Q = 0.01$, $\delta_{iso} = -903$ ppm, $\eta_\delta = 0$, $\Delta_\delta = 0$ ppm, $\nu_r = 30$ kHz. The satellite transitions ($\pm 3/2 \leftrightarrow \pm 5/2$), ($\pm 3/2 \leftrightarrow \pm 1/2$) and the central transition ($\pm 1/2 \leftrightarrow \pm 1/2$) together with simulations are shown on the right and the left sides of the main spectrum.

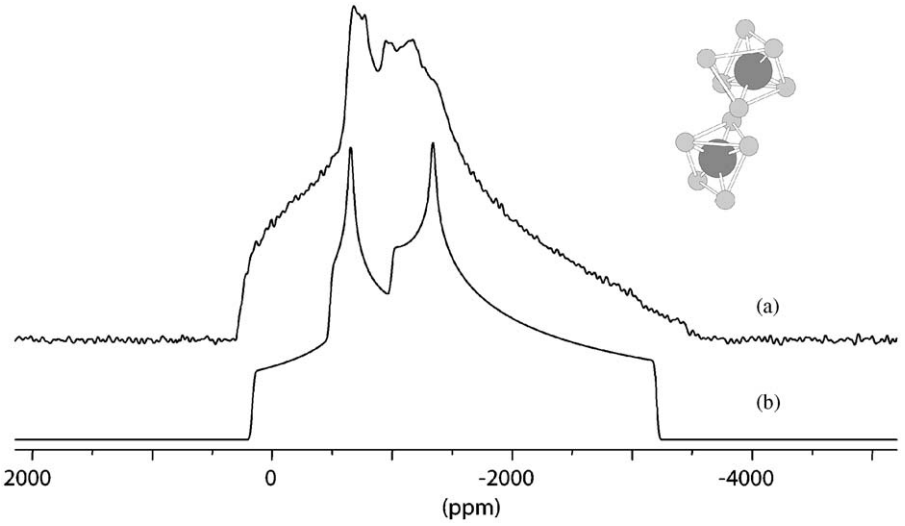

Fig. 21. (a) Experimental ^{93}Nb static spectrum of $CaNb_2O_6$ obtained with a quadrupole solid-echo sequence at 9.4 T. (b) Simulated ^{93}Nb static spectrum at 9.4 T with parameters: $C_Q = 50$ MHz, $\eta_Q = 0.8$, $\delta_{iso} = -990$ ppm, $\eta_\delta = 0.5$, $\Delta_\delta = -300$ ppm. Structure of $CaNb_2O_6$ is shown in the right upper corner. Each niobium octahedron shares two edges with adjacent niobium octahedra forming chains. One Nb–O distance in niobium octahedra is very long (2.34 Å), therefore the effective coordination number of Nb is five.

of niobium octahedra are oriented along the *c*-axis and are connected to each other via calcium atoms. Because one of the distances in niobium octahedra is too long (2.342 Å), the effective coordination number of Nb is five [61].

^{93}Nb NMR spectra of $CaNb_2O_6$, as well as calculated NMR parameters are in agreement with its structure (Figs. 21 and 22). Thus, the isotropic shift of ~−990 ppm is typical for five-coordinated sites (or six-coordinated with cubic symmetry, but since $CaNb_2O_6$ has the orthorhombic symmetry, this shift should be attributed to five-coordinated sites), whereas large C_Q~50 MHz is caused by pseudo-octahedral structure, where one of the Nb–O distances is too long (the same is also true for

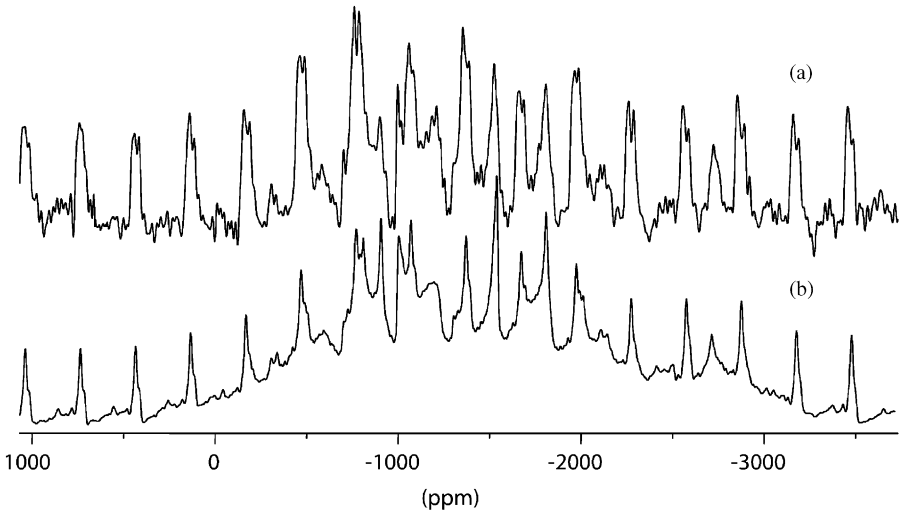

Fig. 22. (a) Experimental ^{93}Nb MAS spectrum of $CaNb_2O_6$ obtained at 9.4 T using a 2.5 mm MAS probe ($\nu_r = 35$ kHz). (b) Simulated ^{93}Nb MAS spectrum at 9.4 T with the following parameters: $C_Q = 50$ MHz, $\eta_Q = 0.8$, $\delta_{iso} = -990$ ppm, $\eta_\delta = 0$, $\Delta_\delta = -100$ ppm, $\nu_r = 35$ kHz.

pseudo-tetrahedral coordination in $MNbO_4$, when two Nb–O distances are too long).

Therefore, the following ^{93}Nb NMR features have been revealed for five-coordinated Nb sites. In comparison with four- and six-coordinated sites, five-coordinated Nb demonstrates an intermediate range of the isotropic chemical shifts. The quadrupole coupling constant depends on the local symmetry: it is small for symmetric isolated sites, and large for pseudo-octahedral sites with one long Nb–O bond.

3.5. Seven- and eight-coordinated compounds

$LaNb_5O_{14}$: $LaNb_5O_{14}$ is orthorhombic, space group *Pbcm*. The structure consists of three types of NbO_x polyhedra: edge-sharing pentagonal NbO_7 bipyramids forming chains, which are interconnected by corner-sharing NbO_6 octahedra. This unusual arrangement of NbO_6 and NbO_7 polyhedra creates channels containing lanthanum ions [62].

^{93}Nb NMR spectra for this compound are very complicated due to presence of three different Nb sites with lines strongly overlapped. To obtain reliable ^{93}Nb NMR parameters for all three sites we have applied the high-field DQ STMAS technique, which is more efficient in this case than MQMAS. The ^{93}Nb DQ STMAS spectrum of $LaNb_5O_{14}$ is shown in Fig. 23. In agreement with crystallographic data, there are three components in this spectrum with isotropic shifts at −1200, −1230 and −1267 ppm, corresponding to two octahedral NbO_6 and one NbO_7 polyhedron, respectively. These three sites are populated as 8:8:4, i.e. the relative number of NbO_7 sites is significantly lower, that is why the dominating in the ^{93}Nb NMR spectra are the octahedral sites.

$NaNb_3O_8$: $NaNb_3O_8$ also forms a channel structure comprised of two types of chain-forming niobium polyhedra, edge-sharing NbO_8 dodecahedra (Nb–O distances: 2.070×4, 2.081×4 Å) and edge-sharing distorted pentagonal bipyramids NbO_7 parallel to [0 0 1] (Nb–O distances: 1.834, 1.947, 1.948, 1.959, 2.212, 2.367×2 Å). These chains are connected to each other via common edges and corners. This specific chain arrangement leads to formation of channels along the *c*-axis with elongated hexagonal cross-sections. Na^+ ions are located in these channels. High-temperature factors reported for this structure are most likely caused by high mobility of Na^+ ions in the channels [63].

Due to complicated synthesis of this compound and its instability, we were unable to perform ultrahigh field ^{93}Nb NMR experiments. At lower fields (9.4 T) it was very difficult to determine accurate ^{93}Nb NMR parameters for two non-equivalent Nb sites. The ^{93}Nb NMR static spectra were very broad to distinguish two individual components with typical second-order features of the central transitions. Nevertheless, it was clear that these spectra were indeed a superposition of at least two subspectra, both strongly shifted up-field. From the high-speed ^{93}Nb MAS spectra (not shown) it was possible to estimate the isotropic shifts for both Nb sites. Thus, for seven-coordinated niobium sites the isotropic shift was found at ca. −1250 ppm and for eight-coordinated niobium sites at −1500 ppm.

We may conclude that compared to six-coordinated niobium, seven- and eight-coordinated Nb sites demonstrate high-field shifts, while the magnitude of the quadrupole coupling constant is mostly determined by the local symmetry.

4. ^{93}Nb NMR chemical shift scale

Combination of the conventional and ultrahigh field NMR measurements with ultrahigh speed MAS, DQ

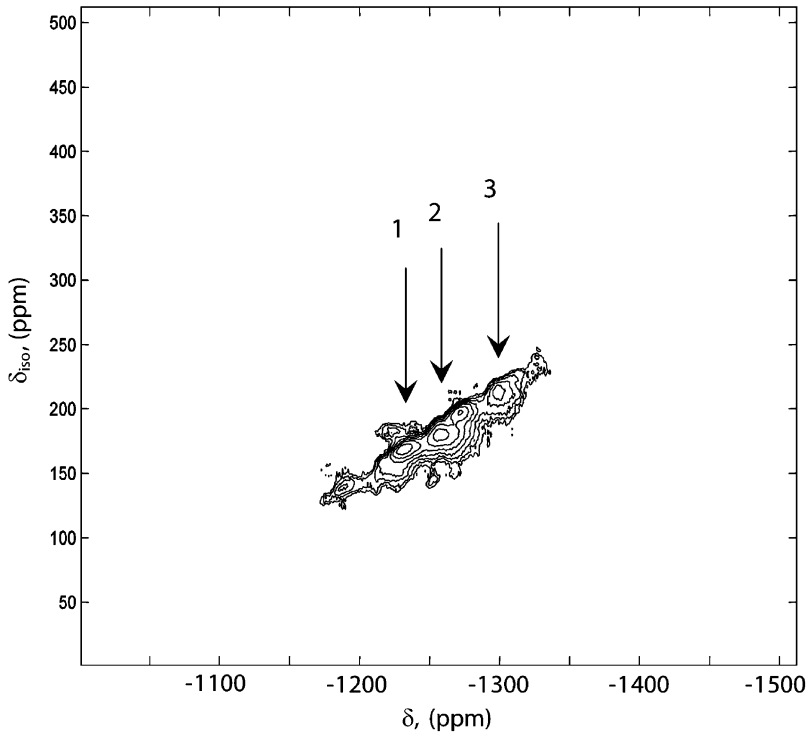

Fig. 23. ^{93}Nb DQ STMAS spectrum of $LaNb_5O_{14}$ obtained at 21.14 T ($\nu_r = 20$ kHz). Three non-equivalent Nb sites are indicated (1, 2, 3).

STMAS, solid-echo techniques and computer modeling allowed us to determine the chemical shift and the quadrupole tensor parameters for a considerable number of Nb compounds (Table 1). We have been able to identify several common ^{93}Nb NMR features.

For four-coordinated Nb sites, the isotropic chemical shifts, corrected for the second-order quadrupole perturbations, occur from −650 to −950 ppm, $C_Q > 70$ MHz.

For five-coordinated Nb sites the isotropic chemical shift changes in the range from −920 to −990 ppm, $C_Q \sim 10$ to 50 MHz, $\Delta_\delta \sim 200$ ppm.

For six-coordinated Nb sites the isotropic shift δ_{iso} varies from −900 to −1300 ppm, C_Q from 1 to 100 MHz, Δ_δ from 0 to 300 ppm. The range of −900 to −1000 ppm is typical for cubic symmetry. For six-coordinated Nb sites with non-cubic symmetry, the ^{93}Nb isotropic chemical shifts are influenced by the ionic character of the niobium sublattice. In niobates of M(+1, +2, +3) elements the niobium sublattice has more anionic character, and the isotropic shifts are in the range from −1000 to −1100 ppm. When M(+4) or M(+5) is present, the niobium sublattice has more cationic character and the isotropic chemical shifts are at −1200 to −1300 ppm. The value of the quadrupole coupling constant for six-coordinated Nb sites varies in a wide range and depends on the site symmetry. The CS anisotropy is well pronounced only when atoms other than oxygen are present in the first coordination sphere, for example, F.

For seven-coordinated niobium sites the isotropic shift varies from −1200 to −1600 ppm. And for eight-coordinated niobium sites the isotropic shift occurs at fields higher than −1500 ppm.

Recently, Grey and coauthors have suggested that a possible correlation may exist between the local structure (coordination) of Nb sites and C_Q values [39,40]. They have speculated that C_Q should increase upon transition from the cubic environment through the pseudo-octahedral and heptacoordinated environments to the pentacoordinated niobium sites. They observed that C_Q was very small in NbO_2F (several hundreds of kHz), 2.25 MHz in η^5-$C_5H_5Nb(CO)_4$, 19–20 MHz in alkali niobates, and very large (~115 MHz) in NbF_5 and ~40 MHz in K_2NbF_7. However, according to the available structural data, in all these compounds niobium remains six coordinated (with the exception of K_2NbF_7). The only definite conclusion, which could be drawn from these earlier observations, is that for six-coordinated niobium sites the quadrupole coupling constant C_Q can vary in a very wide range, from almost zero to more than 100 MHz. We have also observed similar effects for many Nb compounds.

Our present ^{93}Nb NMR data combined with results published earlier clearly demonstrate that only the ^{93}Nb isotropic chemical shift is sensitive to the niobium coordination number. On this basis the ^{93}Nb NMR chemical shift scale can be proposed for niobium compounds (Fig. 24). This chemical shift scale may prove useful to further advance our understanding of the local Nb environment in Nb-containing systems and catalysts, the origin of the short-range chemical ordering and possible motional behavior of Nb ions.

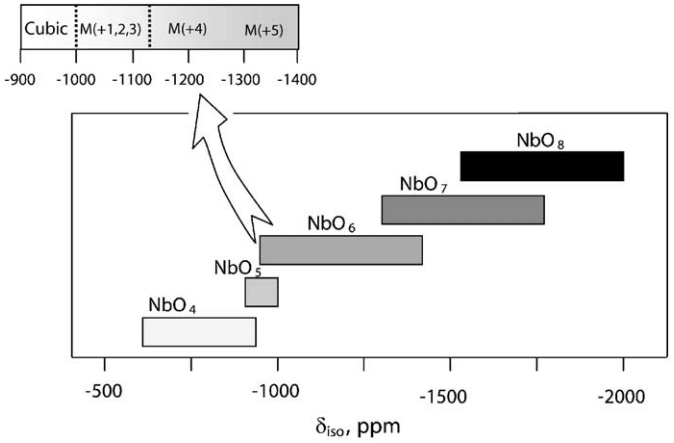

Fig. 24. ^{93}Nb NMR chemical shift scale for NbO_x polyhedra.

Acknowledgments

This work was in part supported by RFBR (Grant #04–03–33070), by SB-FEB-RAS (Grant #48), and by NATO CLG (Grant # ESP.NR.NRCLG 981857). We would like to thank Prof. J.-B. d'Espinose (Laboratoire de Physique Quantique, UMR CNRS, France) for his help with high-field NMR experiments; Prof. A. Shubin and Dr. I. Yudaev (Boreskov Institute of Catalysis, Russia) and Dr. V. Terskikh (University of Ottawa, Canada) for important discussions. The high-speed MAS equipment was provided by Bruker.

References

[1] M.A. Banares, I.E. Wachs, R.M. Martin-Aranda (Eds.), in: Fourth International Symposium on Group Five Compounds, Book of Abstract, Toledo, Spain, 2002.
[2] I.E. Wachs (Ed.), in: Fifth International Symposium on Group Five Compounds, Jiminy Peak, USA, 2005.
[3] K. Tanabe, Catal. Today 78 (2003) 65–77.
[4] M. Ziolek, I. Nowak, Catal. Today 78 (2003) 543–553.
[5] K.J.D. MacKenzie, M.E. Smith, Multinuclear Solid State NMR of Inorganic Materials, Pergamon, Oxford, 2002.
[6] G.E. Peterson, J.R.J. Carruthers, J. Solid State Chem. 1 (1969) 98–99.
[7] G.E. Peterson, A. Carnevale, J. Chem. Phys. 56 (1972) 4848–4851.
[8] R. Kind, H. Granicher, Solid State Commun. 6 (1968) 439–440.
[9] E.N. Ivanova, A.V. Yatseako, N.A. Sergeev, Solid State Nucl. Magn. Reson. 4 (1995) 381–385.
[10] Y. Watanabe, T. Sota, K. Suzuki, N. Iyii, K. Kitamura, S. Kimura, J. Phys.: Condens. Matter. 7 (1995) 3627–3635.
[11] J. Blümel, E. Born, T. Metzger, J. Phys. Chem. Solids 55 (1994) 589–593.
[12] A.F. McDowell, M.S. Conradi, J. Haase, J. Magn. Reson. 119 (1996) 211–218.
[13] F. Wolf, D. Kline, H.S. Story, J. Chem. Phys. 53 (1970) 3538–3543.
[14] J. Davis, D. Tinet, J.J. Fripiat, J.M. Amarillo, B. Casal, E. Ruiz-Hitzky, J. Mater. Res. 6 (1991) 393–400.
[15] A.L. Pomce, X. Lin, J.J. Fripiat, Solid State Ionics 84 (1996) 213–217.
[16] S. Hardin, D. Hay, M. Millikan, J.V. Sanders, T.W.A. Turney, Chem. Mater. 3 (1991) 977–998.
[17] K. Kato, C. Zheng, J.M. Finder, S.K. Dey, Y. Torii, J. Am. Ceram. Soc. 81 (1998) 1869–1875.
[18] A.H. Munhoz, S. Rodrigues, T. Pinnavaia, J. Adv. Sci. Technol. 16 (1999) 521–528.
[19] L.P. Cruz, J.-M. Savariault, J. Rocha, J.-C. Jumas, J.D. Pedrosa de Jesus, J. Solid State Chem. 156 (2001) 349–354.
[20] H. Yoshida, H. Nishihara, S. Yokota, M. Ohyanagi, T. Nakaoki, Z. Naturforsch. A: Phys. Sci. 53 (1998) 309–313.
[21] J. Rocha, P. Brandao, Z. Lin, A.P. Esculcas, A. Ferreira, M.W. Anderson, J. Phys. Chem. 100 (1996) 14978–14983.
[22] K.O. Drake, D. Carta, L.J. Skipper, F.E. Sowrey, R.J. Newport, M.E. Smith, Solid State Nucl. Magn. Reson. 27 (2005) 28–36.
[23] M.J. Duer, Solid-State NMR Spectroscopy Principles and Applications, Blackwell Science Ltd., UK, 2002.
[24] A. Samoson, E. Lippmaa, A. Pines, Mol. Phys. 65 (1988) 1013.
[25] K.T. Mueller, B.Q. Sun, G.C. Chingas, J.W. Zwanziger, T. Terao, A. Pines, J. Magn. Reson. 86 (1990) 470–487.
[26] L. Frydman, J.S. Harwood, J. Am. Chem. Soc. 117 (1995) 5367–5368.
[27] A. Samoson, Chem. Phys. Lett. 119 (1985) 29–32.
[28] Zh.H. Gan, J. Am. Chem. Soc. 122 (2000) 3242–3243.
[29] H.-T. Kwak, Zh. Gan, J. Magn. Reson. 164 (2003) 369–372.
[30] A. Samoson, E. Lippmaa, Chem. Phys. Lett. 100 (1983) 205–208.
[31] D. Massiot, V. Montouillout, F. Fayon, P. Florian, C. Bessada, Chem. Phys. Lett. 272 (1997) 295–300.
[32] F.H. Larsen, H.J. Jakobsen, P.D. Ellis, N.C. Nielsen, J. Magn. Reson. 131 (1998) 144–147.
[33] J.J. Fitzgerald, S. Prasad, J. Huang, J.S. Shore, J. Am. Chem. Soc. 122 (2000) 2556–2566.
[34] S. Prasad, P. Zhao, J. Huang, J.J. Fitzgerald, J.S. Shore, Solid State Nucl. Magn. Reson. 14 (1999) 231–235.
[35] L.P. Cruz, J. Rocha, J.D. Pedrosa de Jesus, J.M. Savariault, J. Galy, Solid State Nucl. Magn. Reson. 15 (1999) 153–158.
[36] S. Prasad, P. Zhao, J. Huang, J.J. Fitzgerald, J.S. Shore, Solid State Nucl. Magn. Reson. 19 (2001) 45–62.
[37] J.J. Fitzgerald, J. Huang, H. Lock, Piezoelectric Materials: Advances in Science, Technology and Applications, vol. 76, NATO Sci. Ser. 3, Kluwer Academic Publishers, Dordrecht, 2000, pp. 203–218.
[38] R. Blinc, A. Gregorovic, B. Zalar, R. Pirc, V.V. Laguta, M.D. Glinchuk, J. Appl. Phys. 89 (2001) 1349–1354.
[39] L.-S. Du, R.W. Schurko, N. Kim, C.P. Grey, J. Phys. Chem. A 105 (2001) 760–768.
[40] L.-S. Du, R.W. Schurko, N. Kim, C.P. Grey, J. Phys. Chem. A 106 (2002) 7876–7886.
[41] Ph.R. Bodart, J.-P. Amoureux, Y. Dumazy, R. Lefort, Mol. Phys. 98 (2000) 1545–1551.
[42] S.E. Ashbrook, S. Wimperis, J. Magn. Reson. 156 (2002) 269–281.
[43] J.P. Amoureux, L. Delevoye, S. Steuernagel, Zh. Gan, S. Ganapathy, L. Montagne, J. Magn. Reson. 172 (2005) 268–278.
[44] A.A. Shubin, O.B. Lapina, G.M. Zhidomirov, IXth AMPERE Summer School, Abstracts, Novosibirsk, 1987. p. 103.
[45] D. Massiot, F. Fayon, M. Capron, I. King, S. Le Calve, B. Alonso, J.-O. Durand, B. Bujoli, Zh. Gan, G. Hoatson, Magn. Reson. Chem. 40 (2002) 70–76.
[46] K. Ukei, H. Suzuki, T. Shishido, T. Fukuda, Acta Crystallogr. C 50 (1994) 655–656.
[47] T. Shishido, H. Suzuki, K. Ukei, T. Hibiya, T. Fukuda, J. Alloys Compounds 234 (1996) 256–259.
[48] M.A. Subramanian, J.C. Calabrese, Mater. Res. Bull. 28 (1993) 523–529.
[49] R. Hsu, E.N. Maslen, D. Du Boula, N. Ishizawa, Acta Crystallogr. B 53 (1997) 420–428.
[50] M.D. Meadows, K. A Smith, R.A. Kinsey, M. Rothgeb, R.P. Skarjune, E. Oldfield, Proc. Natl. Acad. Sci. USA 79 (1982) 1351–1355.
[51] A.W. Hewat, J. Phys. C 6 (1973) 2559–2572.
[52] V.A. Shuvaeva, M. Yu. Antipin, Kristallografiya 40 (1995) 511–516.
[53] A.C. Sakowski-Cowley, K. Lukaszewicz, H.D. Megaw, Acta Crystallogr. B 25 (1969) 851–865.
[54] T.S. Ercit, P. Cerny, Can. Mineral. 26 (1988) 899–903.
[55] A. Kahn-Harari, L. Mazerolles, D. Michel, F. Robert, J. Solid State Chem. 116 (1995) 103–106.
[56] J. Galy, O. Lindqvist, J. Solid State Chem. 27 (1979) 279–286.

[57] H. Weitzel, H. Schroecke, Z. Kristallogr. 152 (1980) 69–82.
[58] S. Tsunekawa, T. Kamiyama, K. Sasaki, H. Asano, T. Fukuda, Acta Crystallogr. A 49 (1993) 595–600.
[59] N.A. Godina, T.I. Panova, E.K. Keller, Izv. AN SSSR. Inorg. Mater. 5 (1969) 1974–1977.
[60] J. Darriet, A. Maazaz, J.C. Bouloux, C. Delmas, Zeit. Anorg. Allg. Chem. 485 (1982) 115–121.
[61] J.P. Cummings, S.H. Simonsen, Am. Mineral. 55 (1970) 90–97.
[62] R. Hofmann, R. Gruehn, Zeit. Anorg. Allgem. Chem. 590 (1990) 81–92.
[63] K.-J. Range, M. Wildenauer, A.M. Heyns, Angew. Chem. Int. Ed. Engl. 27 (1988) 969–971.
[64] A. Castro, E. Aguado, J.M. Rojo, P. Herrero, R. Enjalbert, J. Galy, Mater. Res. Bull. 33 (1998) 31–41.